INTEGRATED MICROPHOTONIC RECEIVER FOR KA-BAND
FINAL TECHNICAL REPORT

Award number: NAG3-2559

Research Period: March 10, 2001 – March 9, 2005

Organization: University of Southern California

Principal Investigator:
Prof. A.F.J. Levi
Advanced Interconnect and Network Technology
3620 S. Vermont Ave., KAP 132
Los Angeles, CA 90089-2533
voice: (213) 740-7318
fax: (213) 740-9280
email: alevi@usc.edu

USC Contract Administrator:
Ms. Loudes Creus
Dept of Contracts & Grants
University Park - STO 324
Los Angeles, CA 90089-1147
voice: (213) 740-6058
fax: (213) 740-6070
email: creus@usc.edu

FINAL REPORT

Microphotonic RF receiver
Award number: NAG3-2559
Start date: March 10, 2001
End date: March 9, 2005

Outline

This report consists of four main sections:

Part I: $LiNbO_3$ microdisk resonant optical modulator. Brief review of microdisk optical resonator and RF ring resonator. Microwave and photonic design challenges for achieving simultaneous RF-optical resonance are addressed followed by our solutions.

Part II: Experimental demonstration of $LiNbO_3$ microdisk modulator performance in wired and wireless RF-optical links.

Part III: Microphotonic RF receiver architecture that exploits the nonlinear modulation in the $LiNbO_3$ microdisk modulator to achieve direct photonic down-conversion from RF carrier without using any high-speed electronic elements.

Part IV: Ultimate sensitivity of the microdisk photonic receiver and the future road map toward a practical device.

Introduction

The main objective of this project was to design and build a new kind of wireless receiver based on the electro-optic response of a high-Q $LiNbO_3$ microdisk optical resonator.

The key component in this receiver is a very sensitive optical modulator. The high sensitivity is provided by simultaneous RF-optical resonance in an electro-optic microdisk. The microdisk optical resonator provides the spatial confinement and long photon lifetime while a miniature RF resonator generates an amplified electric field around the microdisk. The electric field modulates the refractive index of the microdisk and consequently the intensity of the optical output. The high sensitivity is a result of simultaneous optical and electrical resonance. By optimizing the RF and optical design we were able to build a very sensitive $LiNbO_3$ microdisk modulator for optical modulation in Ku-band. The next challenge was creating a microphotonic receiver architecture that could use the sensitivity of microdisk modulator to replace the high-speed electronic elements used in a conventional RF receiver (including the local oscillator) with photonic devices and low-speed electronics. Based on the idea of nonlinear optical modulation in a microdisk modulator we designed a photonic RF receiver that directly extracts the baseband information from a transmitted carrier RF signal only by using $LiNbO_3$ microdisk modulator and a low-speed photodetector.

Part I:

$LiNbO_3$ microdisk optical resonator

Crystalline Lithium Niobate ($LiNbO_3$) is a commonly used electro-optic material in optical modulators. Its superb optical, electrical and mechanical characteristics such as low loss at RF and optical frequencies, high electro-optic coefficient, mechanical robustness and stable crystal structure at room temperature make $LiNbO_3$ a perfect candidate in many electro-optical devices including microdisk modulators. Some of the relevant opto-electronic properties of bulk $LiNbO_3$ crystal are summarized in Table. 1 [1-4]. The core element of the microdisk modulator is a $LiNbO_3$ microdisk optical resonator that supports very high-Q Whispering-Gallery resonance. The microdisk resonator is fabricated from a z-cut $LiNbO_3$ cylinder. As shown in Fig. 1(a), the basic geometry is a disk of diameter D, and thickness h. For devices presently under test, 0.1 mm< h < 1 mm and 1 mm< D < 6 mm. The sidewall of the disk is optically polished with a radius of curvature R, typically equal to the radius of the disk. In addition, the equator of the disk's sidewall should be accurately maintained at height $h/2$.

Table. 1[1-4]

Property	Value	Notes
Ordinary optical index of refraction (n_o)	2.223	@ 1550 nm
Extraordinary optical index of refraction (n_e)	2.143	@ 1550 nm
RF permitivity along c-axis ($\varepsilon_{RF,e}$)	42.5 - 43	100 MHz - 140 GHz
RF permittivity perpendicular to c-axis ($\varepsilon_{RF,o}$)	26-28	100 MHz - 140 GHz
Electro-optic coefficients (pm/V)	r_{33} = 30.8 r_{22} = 3.4 r_{13} = 8.6 r_{51} = 28.0	
Dielectric loss tangent along c-axis	0.004	

Polishing curved sidewalls to an optical finish in $LiNbO_3$ is not a standard practice and it is very difficult to achieve the surface quality needed for high-Q optical resonance. Using advanced optical polishing techniques we developed a specialized method for optical-quality polishing of the curved sidewalls of $LiNbO_3$ microdisks.

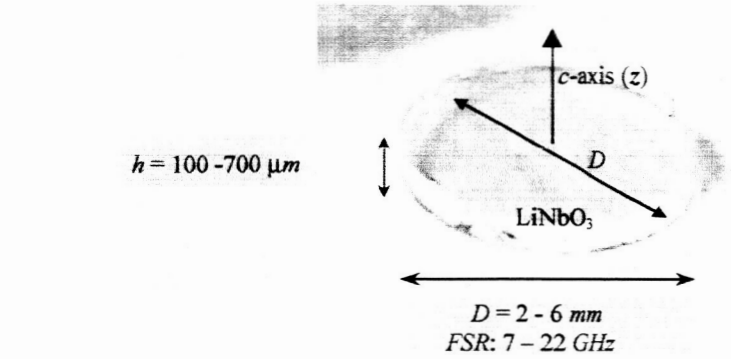

(a)

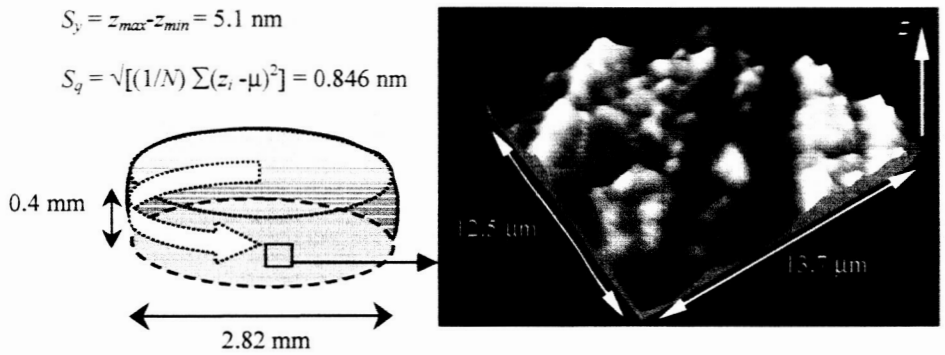

N : Total number of sample points
μ : Mean height

(b)

Figure 1 (a) Photograph of a $LiNbO_3$ disk with optically polished sidewalls. (b) 3D picture of the disk sidewall surface taken by interferometric surface profilometer.

The technology has been transferred to a company (www.opticology.com) and they improved the technique furthermore so that now they are able to make very small (1 mm diameter and 0.150 mm thick) high-Q (>10^6) $LiNbO_3$ microdisk optical resonators.

Fig. 1(b) shows a 3D picture of the sidewall surface roughness for a typical microdisk (taken with *interferometric surface profiler*). The peak-to-peak value (S_y) of surface roughness is about 5.1 nm and its rms value (S_q) is about 0.846 nm. With this surface quality loaded optical-Qs up to 7×10^6 (unloaded Q of about 2×10^7) have been achieved. This corresponds to a distributed loss of less than 0.0075 cm^{-1} (or 0.03 dB/cm). Since $LiNbO_3$ is an electro-optic active material its refractive indices are changed in the presence of an electric field. An E-field with a magnitude E_c along the c-axis changes the optical refractive indices according to:

$$\Delta n_{zz} = n_e^3 \, r_{33} E_c/2 \qquad \Delta n_{xy} = n_o^3 \, r_{13} E_c/2$$

where $r_{33} \approx 30.8 \times 10^{-12}$ m/V and $r_{13} \approx 8.6 \times 10^{-12}$ m/V.

The resonances of a spherical resonator are described in terms of three integer set l, m and q. The value of q counts the number of field maxima in the radial direction and l-m +1 ($|m| \leq l$) is the number of field maxima in the polar direction, perpendicular to equatorial plane and between two poles [5-7]. The resonant frequency ($\nu_{res} = \nu_{l,q}$) is determined by q and l. The mode labeled by $l = m$ and $q = 1$ is called the fundamental Whispering Gallery (WG) mode and it only has one maximum in each direction (and has a Guassian profile).

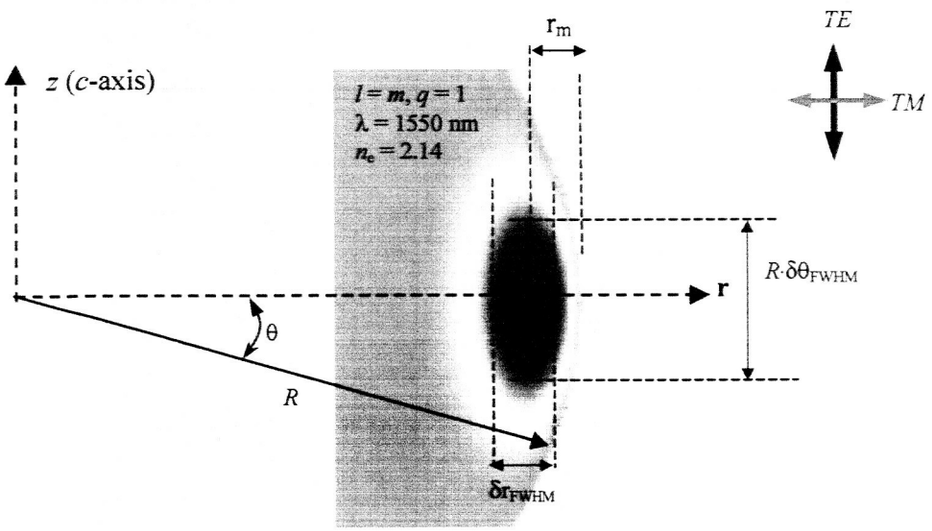

2R (mm)	$R{\cdot}\delta\theta_{FWHM}$ (μm)	δr_{FWHM} (μm)	r_m(μm)	l (= m)
2	17.8	4.06	3.31	8660
3.5	24	4.99	4.00	15120
5.84	30	5.80	4.58	25260

Figure 2 WGM power distribution in xz plane, for microdisks with different diameters [35]. Notice that θ is measured relative to the equatorial plane unlike the conventional definition that is measured relative to z-axis. This new definition has been chosen because it is more convenient for WG resonances that are confined around the equator. Also shown is the definition of the TE and TM polarized resonances relative to c-axis.

Fig. 2 shows the definition of the fundamental mode profile parameters and their values for three $LiNbO_3$ microdisks with different sizes commonly used in our experiments [35]. δr_{FWHM} is the full-width-half-maximum of the power distribution along radial direction and $\delta\theta_{FWHM}$ is the full width half maximum along polar direction.

The resonant frequency of the fundamental Whispering Gallery (WG) and low order resonances can be calculated using the approximation: $m(\lambda_m/n) = \pi D$ (m is the number wavelengths around the periphery of the microdisk and n is the optical index of refraction). Then the optical free spectral range (FSR) frequency $\Delta\nu_{FSR}$ may be calculated using: $\Delta\nu_{FSR} = c/(nD)$.

The optical modes with an *E*-field parallel polarized along the *c*-axis are labeled as TE and those with an *E*-field parallel to the *xy* plane as TM modes. Due to the large magnitude of the electro-optic coefficient along *c*-axis we use TE polarized WG modes for optical modulation.

Assuming the number of photons present in a WG mode decays exponentially in time (intrinsic optical losses) we can express the unloaded optical quality factor of that mode as $Q_u = \omega\tau_p$ where τ_p is the 1/e photon lifetime and $\omega = 2\pi\nu_{l,q}$ (where $\nu_{l,q}$ is the resonant frequency of the mode). We can also define a distributed loss constant per unit length $\alpha = n/c\tau_p$ (c: is the speed of light and n is the effective optical refractive index for the corresponding optical mode). So Q_u and the distributed loss are related as: $\alpha = n\omega/cQ_u$.

The loaded optical quality factor Q of an optical mode can be calculated based on the measured full-width half maximum of the spectral peak at the resonant optical frequency $\nu_{res} = \nu_{l,q}$, $Q = \nu_{res}/\Delta\nu_{FWHM}$ (or $Q = \lambda_{res}/\Delta\lambda_{FWHM}$). The typical Q-factor (loaded) values that we observe for optically polished $LiNbO_3$ micodisks is between 2×10^6 and 7×10^6. Experimentally we measure the loaded Q so if we use the measured value of Q to calculate α, the optical coupling loss will be included in the distributed loss.

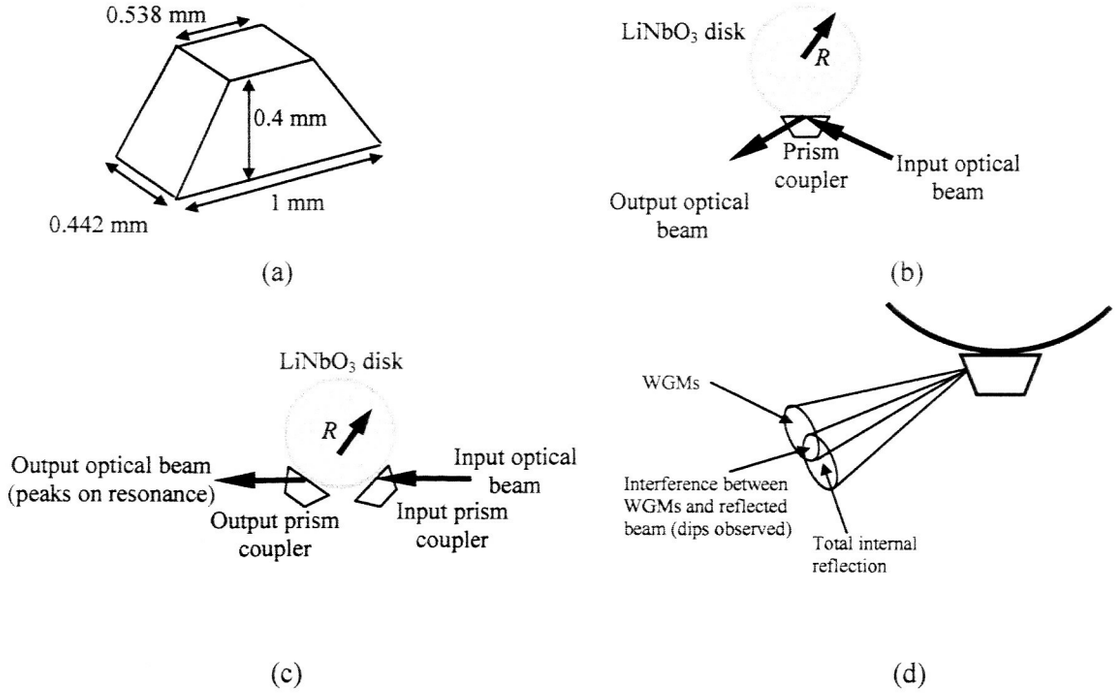

Figure 3 (a) Diamond microprism dimensions. (b) Single-prism coupling. (c) Double-prism coupling. (d) Interference effect in single-prism coupling.

Knowing the loaded quality factor of a critically coupled WG mode we were able calculate the intrinsic distributed loss in the microdisk resonator (~0.0075 cm^{-1}).

In our experiments we use evanescent coupling through small diamond prisms with dimensions shown in Fig. 3(a). The refractive index of diamond is about 2.4 that is larger than the refractive index of $LiNbO_3$ for both TE and TM modes ($n_e = 2.14$, $n_o = 2.23$). It is possible to use a single prism to couple light into and out of the microdisk (Fig. 3(b)) or use one prism to couple in and another one for coupling out (Fig. 3(c)). Detection of coupled WG peaks using two prisms is easier since the reflected (part of the input that is not coupled) and coupled light don't interfere but since two prism are in contact with microdisk the Q is smaller (due to larger coupling loss) and also part of the optical WGM power that is coupled out through the first prism can't be used for modulation. In one-prism coupling scheme this problem doesn't exist but experimental results show that the WGM cone coupled out of the disk and the totally reflected beam cone have spatial overlap (Fig. 3(d)), so depending on the location of the collecting fiber the detected output spectrum can be WGM peaks, transmission dips or just the reflected beam. This effect makes the alignment of the output port more complex. Also experimental results shows generally two-prism coupling results in a cleaner mode structure. Using transmission dips in a one-prism coupling scheme is a better choice for nonlinear modulation and optical down-conversion due to reduced DC optical power at resonance.

Fig. 4(a) shows the close up photographs of the microdisk, the microprisms and the output fiber. Here the double-prism coupling scheme is used. The input light is a laser beam with a wavelength of 1550 nm and a linewidth of less than 500 kHz from a tunable laser source. Due to high-Q nature of the optical resonance a very high resolution tunable laser source is required for accurate tuning of the wavelength relative to the resonant wavelength. The resolution of the laser used in our experiments is less than < 0.3 pm. The laser beam is collimated and then focused on the input microprism through a matched pair lens system with a focal length of 11 mm.

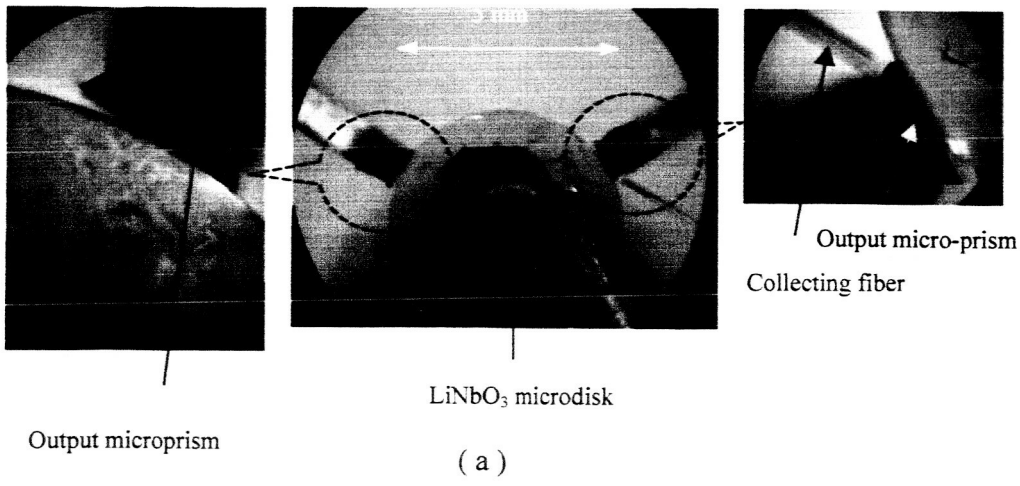

(a)

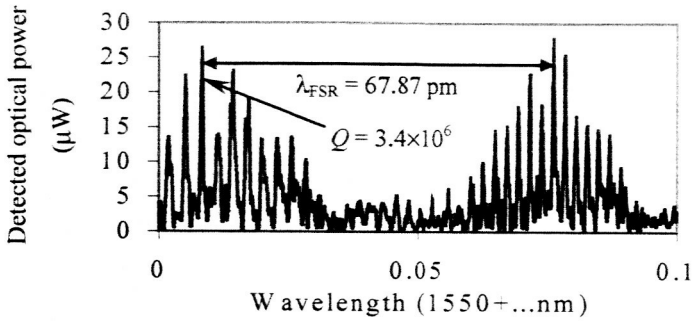

(b)

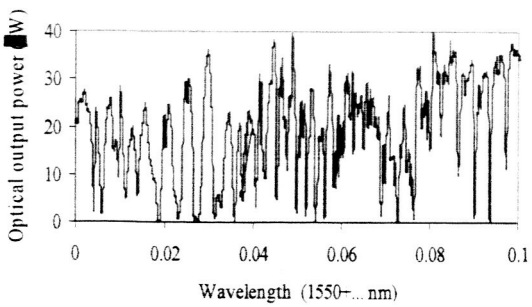

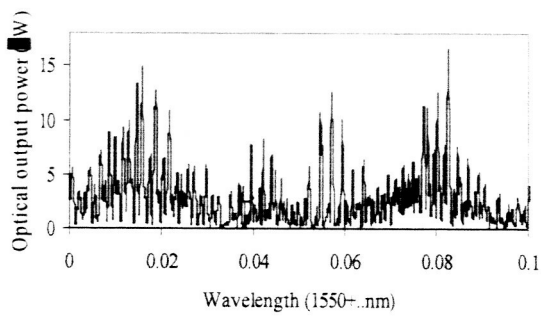

(c) (d)

Figure 4 (a) Photograph of a 5.13 mm diameter $LiNbO_3$ microdisk in contact with two microprisms. (b) The detected TE WG optical output power spectrum. (c) and (d) are the measured optical out power spectrum of a single prism coupled $LiNbO_3$ microdisk (D = 3 mm, h = 0.4 mm). (c) Detected transmission dips when the output fiber is tuned to the overlap region of the WG cone and the total reflection cone. (d) Detected WG peaks when the output fiber only collects optical power from the WG cone.

Fig. 4(b) shows the typical TE optical output spectrum obtained in a double prism configuration. This spectrum is measured using the $LiNbO_3$ microdisk in Fig. 4(a) that has a diameter of 5.13 mm and a thickness of 0.4 mm. The measured FSR is in very good agreement with the calculated value (assuming $n_{eo} = 2.14$). For the 5.13 mm diameter disk the calculated value is 69.24 pm and the measured value is 67.87 pm. This shows the effective refractive index of TE WG modes is almost the same as the bulk extraordinary refractive index (*E*-field along *c*-axis). The maximum optical coupling efficiency observed is about 15% coupling efficiency. Notice that we define the coupling efficiency as the ratio of the resonant optical power of an optical mode and the total power injected to the input prism. As mentioned before using one prism coupling scheme the optical spectrum of the collected output power could be a series of transmission dips or peaks depending on the position of the output fiber. Fig. 4(c) and (d) show the spectrum of the TE optical output power from a single prism coupled $LiNbO_3$ microdisk (D = 3 mm, h = 0.4 mm). In Fig. 4(c) the output fiber is located at the overlap of the WG cone and the totally reflected cone while in Fig. 4(d) it only collects the WG optical power.

DC electro-optic response

Evaluating the DC response of the WG resonances to an external electric field is the first step toward building an microdisk optical modulator.

If we place a conductive ring (with a diameter equal to D) on top of a $LiNbO_3$ microdisk that is mounted on a ground plane then a DC voltage on the ring will generate an *E*-field (mainly along z-direction) around the disk where the WG modes are propagating. Since $LiNbO_3$ is an electro-optic material the *E*-field changes its refractive index and consequently the resonant wavelengths (frequencies) of WG modes. The magnitude of this shift can be estimated as:

$\Delta\lambda_m = \lambda_m n_{eo}^2 r_{33} E_{eff}/2$

Where λ_m is the wavelength of the mth resonant optical mode, E_{eff} is the magnitude of the *E*-field along *z*-axis in the middle of microdisk where the WG mode is traveling. Ideally in the absence of fringing and other perturbing factors the *E*-field intensity in the middle of the disk should be equal to V/h. But due to fringing effect and the air gap between the ring and the microdisk surface the *E*-field intensity inside $LiNbO_3$ is less than the ideal value.

We summarize all these effects and the overlap integral between optical mode and the *E*-field in a correction factor called the optical-mode-electric-field overlap correction factor β_{EO} so:

$E_{eff} = \beta_{EO}(V/h)$. When V = 1 Volt $\Delta\lambda_m$ is called DC shift or $\Delta\lambda_{DC}$. DC shift is an important parameter in a microdisk modulator because it quantifies the electro-optic response of the modulator and is needed for calculating the RF modulation response. The measured value of DC shift for a WG resonance of microdisk can be used to estimate the corresponding β_{EO}. The desired value of β_{EO} should be close to 1 but in most cases it is less than 0.5. β_{EO} is determined by many parameters and it also varies slightly for different WG resonances. It is possible to improve β_{EO} by a geometry that forces the *E*-fields to the optical mode region. In our latest design we mount the microdisk on cylindrical ground plain with the same radius as the disk and we observed a slightly larger DC shift. Fig. 5(a) shows a photograph of the microdisk resonator (D = 3 mm, h = 0.4mm) mounted on a cylindrical ground plane. Fig. 5(b) shows the measured optical output spectrum of the microdisk (shown in Fig. 5(a)) at 0 and 5 Volt DC bias voltage.

The resonator is coupled through a single-prism but the output fiber is tuned to the WG cone to detect the peaks. As may be seen $\Delta\lambda_{DC} = 0.13$ pm (corresponding to $\beta_{EO} = 0.53$).

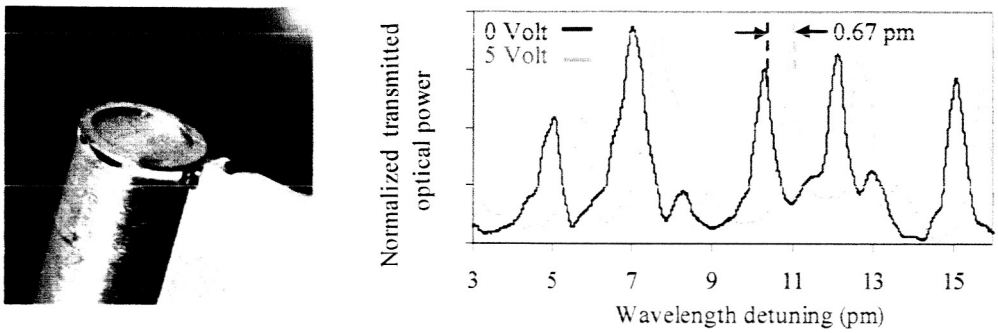

Figure 5 (a) Photograph of the microdisk resonator mounted on a cylindrical ground plane (D = 3 mm, h = 0.4 mm). (b) Measured optical output spectrum at 0 and 5 Volt DC bias voltage.

Optical bistability in microdisk resonator

Bistable optical devices are of the great interest for their possible application to optical computing, optical thresholding and memory [8-10]. As an example of the slow electro-optic response of the microdisk modulator we have demonstrated the bistable behavior of the $LiNbO_3$ microdisk resonator with a feedback loop. This differs from Fabry-Perot case [9] that we are using a traveling was resonator. The reason for our interest is that high-Q should, in principle, make a sensitive device. The microdisk resonator has a diameter of 5.8 mm and a thickness of 0.74 mm. The measured DC shift for this configuration is about 0.09 pm/V. The experimental arrangement to measure electro-optic non-linearity is shown in Fig. 6(a). The voltage applied to the electrode is a function of resonator optical output power. Optical input power to the resonator is provided by a frequency-stabilized laser diode whose output is intensity modulated to create a 500 Hz triangle wave. Optical output power is detected using a photodiode. To study electro-optic bistability, amplified detector output voltage is fed back to the disk electrode. Fig. 6(b) shows the measured optical output-power as a function of optical input-power for the indicated values of peak-to-peak voltage feed-back, V_{fb} and optical Q-factor. The electro-optic system shows a slight non-linearity when $V_{fb} = 1.5\ V_{pp}$, using an optical mode with $Q = 7.5\times10^5$, and significant bistability and hysteresis behavior when $V_{fb} = 3.0\ V_{pp}$, using an optical mode with $Q = 10^6$.

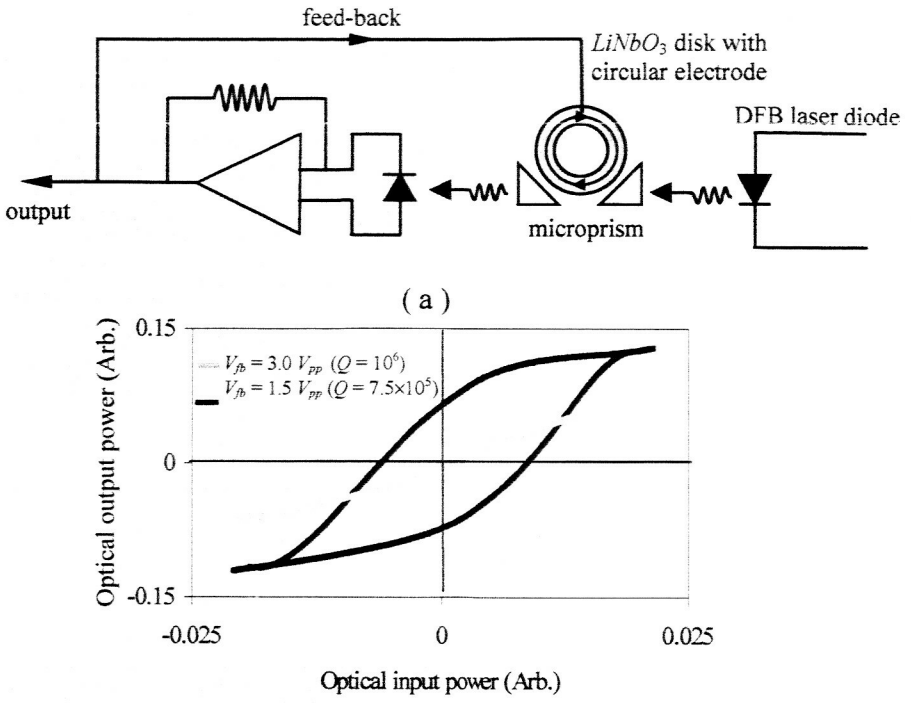

Figure 6 (a) Experimental arrangement used for demonstrating the bistable behavior of the microdisk optical resonator with a feed-back loop. (b) Measure optical output-power as a function of optical input-power for indicated values of peak-to-peak voltage feedback (V_{fb}) and optical Q-factor

Resonant electro-optic modulation in a microdisk modulator

In a resonant optical modulator such as microdisk modulator electro-optical interaction is enhanced through amplified E-field and longer electro-optic interaction length. Optically resonant modulators can only perform efficient modulation within limited bandwidth around discrete RF center frequencies defined by integer multiples of optical free spectral range. Operation in simultaneous electrical and optical resonance operation requires a resonant RF equal to the optical FSR or an integer multiple of the FSR. The modulation bandwidth is limited by the highest quality factor (which in most cases we will consider is the optical Q).

It is important to mention that in optically resonant modulators (unlike MZ modulators) V_π is not a well-defined quantity since the device does not work based on MZ interference principle. Instead there is a Lorentzian transfer function whose resonant wavelength changes as a function of applied electric field. In this case the voltage V_{FWHM} required to shift the resonance by $\Delta\nu_{FWHM}$ (where $\Delta\nu_{FWHM} = Q/\nu_{res}$, ν_{res}: optical resonant frequency) may be used to quantify the modulator performance. Another definition used as a measure of modulator sensitivity is the variation of the optical intensity with respect to voltage at the half-transmission point: $\left.\frac{dP_{o,out}}{dV}\right|_{1/2}$.

For a MZ modulator this quantity is related to V_π by: $V_\pi = \frac{\pi}{2}\left(\left.\frac{dP_{o,out}}{dV}\right|_{1/2}\right)^{-1}$ [11].

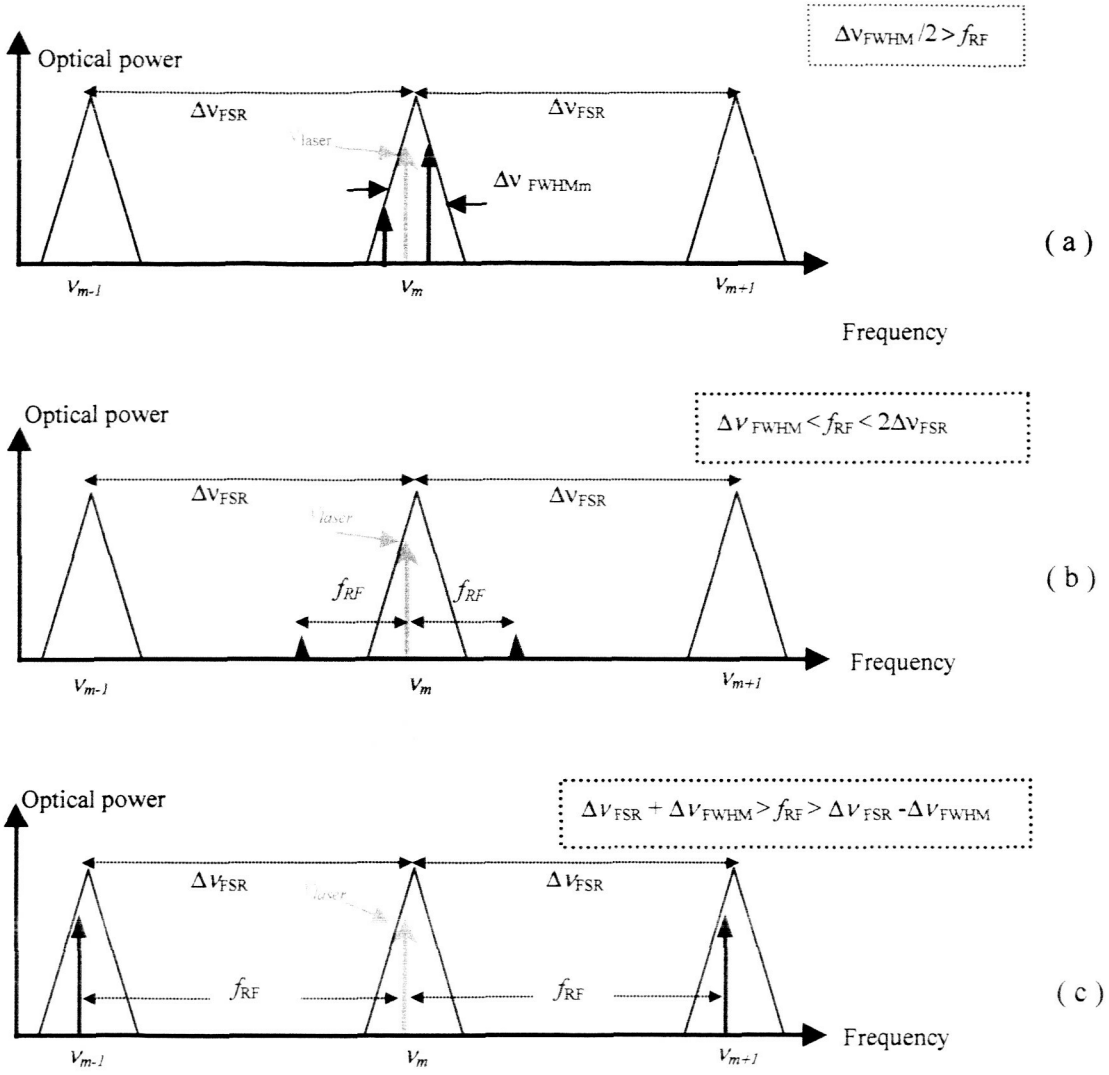

Figure 7 Qualitative behavior of the frequency response based. (a) Linewidth modulation: the RF carrier frequency is smaller than $\Delta\nu_{FWHM}/2$. Polymer and semiconductor microring and microring resonators work in this regime. (b) No modulation: the RF frequency is larger than optical bandwidth but smaller than the optical free-spectral-range so the RF-optical sidebands are filtered out by the optical transfer function. (c) FSR modulation: The RF-optical sidebands are within the adjacent resonances. ($LiNbO_3$ microdisk modulator works in this regime).

This relation can be used to define an equivalent V_π^{eq} for a resonant modulator. If one uses the bandwidth/voltage ratio (f_{3dB}/V_π^{eq}) as the figure of merit for an electro-optic modulator, traveling wave MZ modulators outperform resonant modulators [11]. Although using f_{3dB}/V_π^{eq} as a figure of merit is a reasonable choice for broadband optical communication applications, it is not a suitable choice for RF-subcarrier optical links where a limited bandwidth around a high-frequency carrier is usually required.

The modulation bandwidth of an optically resonant modulator is limited by spectral linewidth and the free spectral range. Using the optical transmission spectrum of the modulator, the modulation spectrum can be qualitatively explained as follows: The optical transmission spectrum of the modulator is a series of equally spaced Lorentzians with linewidths of $\Delta\nu_{FWHM}$ ($\Delta\nu_{FWHM} = Q/\nu_{res}$) separated by $\Delta\nu_{FSR}$ as shown in Fig. 7 ($\Delta\nu_{FSR} = c/\pi D n_e = 1/\tau_{rt}$. τ_{rt} = optical roundtrip time of the resonator).

Through the modulation process optical power is coupled out from ν_{laser} (optical carrier frequency) into optical sidebands $\nu_{laser} \pm f_{RF}$. All of these frequencies ($\nu_{laser} \pm f_{RF}$, ν_{laser}) have to be resonant inside the microdisk so that optical energy cannot be pumped into them. The optical transmission spectrum can be used as a filter that modifies the optical spectrum of the modulated signal. Assuming the laser frequency is tuned to $\nu_m - \Delta\nu_{FWHM}/2$ (middle of the slope), when $f_{RF} \leq \Delta\nu_{FWHM}/2$ both sidebands would be inside the m-th resonance so the output will be modulated (Fig. 7(a)).
As we increase f_{RF} the optical power in the sidebands decreases until they are completely filtered out (Fig. 7(b)). So low frequency modulation is allowed with a bandwidth of about $\Delta\nu_{FWHM}/2$. If we continue increasing f_{RF}, at $f_{RF} \approx \Delta\nu_{FSR}$ again the sidebands become resonant (Fig. 7(c)). It is obvious that since the spectral linewidth is $\Delta\nu_{FWHM}$, the modulation bandwidth around $\Delta\nu_{FSR}$ is $\Delta\nu_{FWHM}$. The same situation is periodically repeated around $f_{RF} = m \times \Delta\nu_{FSR}$ (m is an integer).
We may conclude that only RF frequencies less than $\Delta\nu_{FWHM}/2$ and within a $\Delta\nu_{FWHM}$ bandwidth centered around integral multiples of the optical FSR can modulate the optical mode. We refer to the low frequency modulation as *linewidth* modulation and the modulation at $m \times \Delta\nu_{FSR}$ ($m \neq 0$) as FSR modulation.

Fig. 8(a) shows the ideal frequency response of a resonant optical modulator (solid line) and a traveling wave optical modulator (dashed line).

In both cases we assume the RF and optical waves are phase matched and the high frequency response of the modulator is limited by electrical losses. We should point out that here we want to have a qualitative estimation of the modulation and the details strongly depend on the specific modulator design. As may be seen at high-frequencies where the sensitivity of the traveling wave modulator is reduced we expect better sensitivity from the resonant modulator, even though within a small bandwidth around $m_0 \times \Delta\nu_{FSR}$. The bandwidth limitation imposed by $\Delta\nu_{FWHM}$ and $\Delta\nu_{FSR}$ may challenge the usefulness of employing high-Q resonant modulators for broadband optical communications where data rates as high as 40 Gb/s are currently achieved by traveling wave modulators.

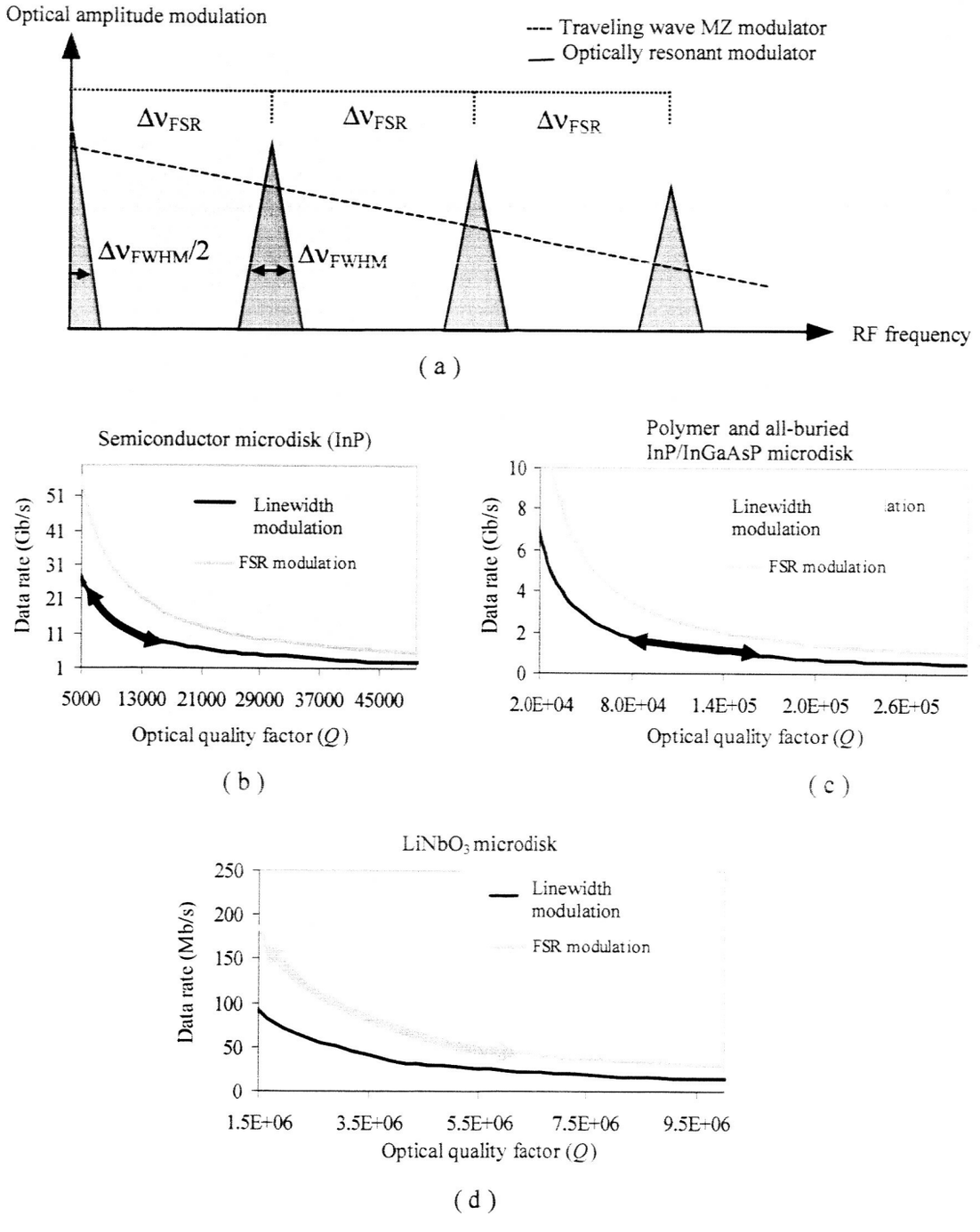

Figure 8 (a) Ideal frequency response of a resonant optical modulator (solid line) and a traveling wave optical modulator (dashed line). (b), (c) and (d) Digital modulation bandwidth of microdisk modulator against optical quality factor in baseband and FSR modulation regimes.

However in most RF-subcarrier links and also wireless communications broadband is unnecessary. In such circumstances resonant microdisk modulators offering efficient modulation around a high frequency carrier may represent a competitive technology. Since the center frequencies ($m_o \times \Delta\nu_{FSR}$) are determined by the refractive index and the diameter of the disk, the RF carrier frequency imposes limitation on the disk size and the electro-optic material. For example Fig. 8(b) and (c) shows that for current wireless applications, where the carrier frequency is between 1 GHz 1 and 60 GHz, the small size polymer and semiconductor microdisks cannot be used for FSR modulation because their FSR is in THz regime. In contrast, the FSR of the average size $LiNbO_3$ microdisks is about 5 to 50 GHz and so is suitable for many wireless applications (Fig. 8(d)).

RF resonator

The key characteristics of the modulating *E*-field for an efficient electro-optic interaction with WG modes inside the disk may be summarized as:

1) Oscillation frequency equal to $m_o \times \Delta\nu_{FSR}$
   (m_o is an integer representing the order optical modulation)
2) Proper spatial distribution.
3) Large interaction length.
4) Large magnitude.
5) Good overlap with the optical mode (large β_{EO}).

The role of an ideal RF resonator is to generate an *E*-field that satisfies all these requirements. As mentioned in the previous section for simultaneous RF and optical resonance in a microdisk modulator the RF resonant frequency should be equal to $m_o \times \Delta\nu_{FSR}$. We refer to this condition as *RF-optical frequency matching* condition (f_{RF} is the RF resonant frequency).

The proper spatial distribution, large interaction length and large magnitude of the *E*-field around the microdisk are required to maximize the electro-optical phase shift at each photon round trip. A microstrip ring resonator on top of the microdisk can fulfill all of these requirements with minimum complexity. It is very important to notice that in a conventional Mach-Zehnder (MZ) modulator both optical and electrical waves are traveling along an open linear trajectory and they are velocity matched for broadband operation. In contrast in a microdisk modulator the optical wave is a resonant traveling wave that circulates around the microdisk. Given the large difference between the RF resonant wavelength, $\lambda_{RF} = c/(n_{RF,e} \times \Delta\nu_{FSR})$ ($n_{RF,e}$ is the effective RF refractive index for the corresponding resonance), and resonant optical wavelength, $\lambda_{res} = c/(n_e \nu_{res})$ the RF field becomes a standing wave. . Fig. 9(a) shows a schematic diagram of the microdisk modulator that employs a ring resonator. The ring is placed on the $LiNbO_3$ microdisk and is side-coupled to a microstripline. Fig 9(b) shows a photograph of our latest experimental arrangement. The microdisk has an FSR of 14.6 GHz and its dimensions and ground plane geometry are the same as Fig. 5.

When a ring resonator is strongly coupled to a microstripline (small gap sizes) the symmetry breaks due to the proximity of the microstripline to the ring and two configurations are possible depending on whether induced magnetic field or induced electric field is maximum at the resonator near the microstripline. The broken symmetry splits each mode into two modes with slightly different resonant frequencies: even and odd modes. Odd modes have lower frequencies and are capacitively coupled to the line, while the even modes have higher frequencies and are

magnetically coupled to the line [14]. The coupling strength dependence on mode order and coupling mechanism results in different loading factors and hence different frequency shifts and loaded Qs. Both even and add modes can be used for optical modulation but since in most cases the resonant frequency of the even mode is closer to $\Delta\nu_{FSR}$ we use even mode.

Because of the large difference between RF and optical refractive index of $LiNbO_3$ ($n_{RF} = 5.1$, $n_e = 2.14$) the main challenge is the RF-optical frequency matching. Using a combination of physical factors that influence the RF resonant frequency of the ring resonator on a dielectric disk (ring dimensions, ring surface roughness and the loading effect) we were able to tune the fundamental resonant frequency ($f_{RF} = f_{RF,1}$) of the side-coupled ring resonator to $\Delta\nu_{FSR}$.

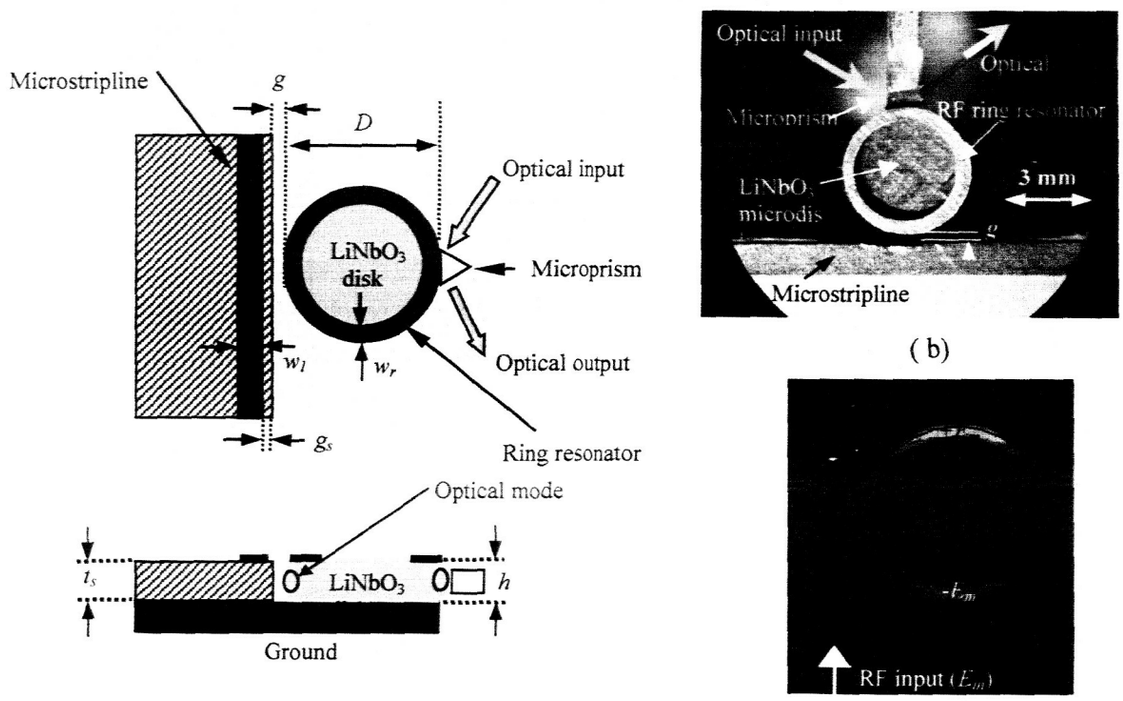

Figure 9 (a) Geometry of ring resonator on $LiNbO_3$ side-coupled to a microstripline (top view and side view) (b) Photograph of our latest experimental arrangement. The microdisk has an FSR of 14.6 GHz and its dimensions and ground plane geometry are the same as Fig. 5(a). (c) Simulated E-field distribution on the equatorial plane of the $LiNbO_3$microdisk while the fundamental resonance of the ring resonator is excited.

Fig. 9(c) shows the simulated E-field distribution on the equatorial plane of the $LiNbO_3$ microdisk while the fundamental resonance of the ring resonator is excited. The sinusoidal spatial distribution and RF-optical frequency matching results in a phase matched electro-optic interaction and optimized optical modulation efficiency.

Assuming $f_{RF,1} = \Delta\nu_{FSR}$ then the harmonics of the ring resonator, $f_{RF,m} = m_R \times f_{RF,1}$, may be used for harmonic optical modulation at $m_R \times \Delta\nu_{FSR}$.

The ring resonator performance is mainly evaluated by measuring the *S*-parameters of the coupled microstipline. We have estimated the voltage gain of the ring resonator as a function of measurable parameters in the system:

$$G_V = \frac{V_m}{V_o} = \sqrt{\frac{4hP_{loss}Q_{RF,U}}{\beta_c Z_o \omega_{RF} \varepsilon_{e,RF} \varepsilon_0 A}}$$

where P_{loss} is the loss factor given by:

$$P_{loss} = P_{RF}^{in}\left(1 - |S_{11o}|^2 - |S_{21o}|^2 - 1.5\left(\frac{L_T - 1}{L_T}\right)\right)$$

V_m : Amplitude of the voltage oscillation on the ring resonator
V_o : Amplitude of the input voltage
h : microdisk thickness
$Q_{RF,U}$: Unloaded RF quality factor of the ring resonator
Z_o : Microstripline impedance
β_c : Capacitance correction factor
ω_{RF} : RF frequency
$\varepsilon_{RF,e}$: RF permittivity along *c*-axis
ε_0 : Permittivity of free space
A : Area of the ring resonator
L_T : Microstripline loss factor
P_{RF}^{in} : RF input power
S_{21o} : Measured S_{21} at resonance
S_{11o} : Measured S_{21} at resonance

$Q_{RF,U}$, f_{RF}, S_{21o} and S_{11o} can be derived from measured *S*-parameter spectrum [13]. When S_{11o} = S_{21o} = 50% the ring is critically coupled to the microstripline and G_V is maximized.

Fig. 10(a) is a photograph of the modified opto-mechanical design that enables the accurate control of the RF coupling gap (*g*).

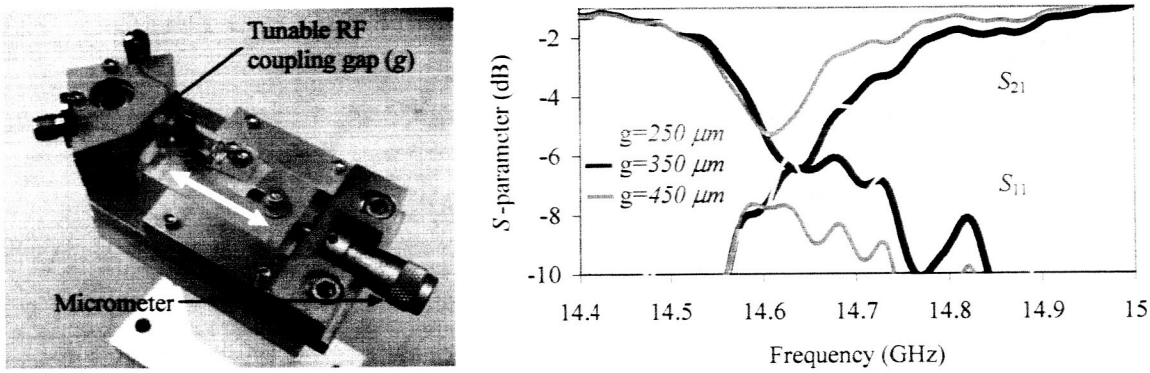

(a) (b)

Figure 10 (a) The optimized opto-mechanical design for tuning the RF coupling. (b) The *S*-parameter measurement results for a ring resonator (w_r = 0.35 mm) on a $LiNbO_3$ microdisk with an FSR of 14.6 GHz (D = 3 mm and t = 0.4 mm) at different values of the gap size (g). At g = 350 μm the critical coupling ($S_{11}^2 = S_{21}^2$ = - 6 *dB*) and RF-optical frequency matching ($f_{RF} = \Delta\nu_{FSR}$ = 14.65 GHz) are achieved simultaneously. Notice that the conventional definition of *S*-parameter is based on voltage ratios but the measured values on network analyzer are power ratios (measured in dB). At g = 250 μm and the resonator is overcoupled and at g = 450 μm is undercoupled.

Fig 10(b) shows The *S*-parameter measurement results for a ring resonator (w_r = 0.35 mm) on a $LiNbO_3$ microdisk with an FSR of 14.6 GHz. As may be seen the RF critical coupling (S_{11o} =

S_{21o}) and RF-optical frequency matching (f_{RF} = $\Delta\nu_{FSR}$ 14.65 GHz) are achieved simultaneously. The estimated value of G_v for this ring resonator is between 5-5.5.

Fundamental single frequency modulation

The modulation efficiency and other characteristics of the microdisk modulator can be measured in a single frequency experiment at f_{RF} = $\Delta\nu_{FSR}$. We used our optimized Ku-band modulator to demonstrate the sensitivity of RF-optical resonant modulator at 14.55 GHz. The microdisk modulator arrangement is shown in Fig. 11(a).

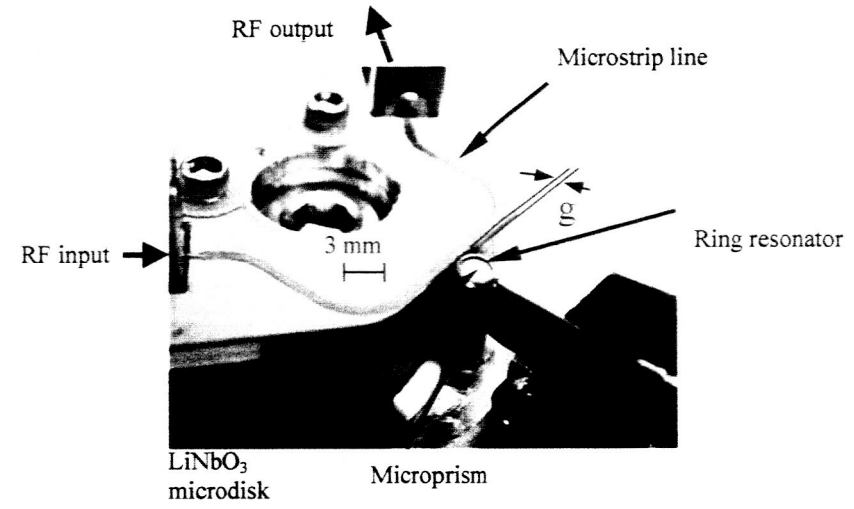

(a)

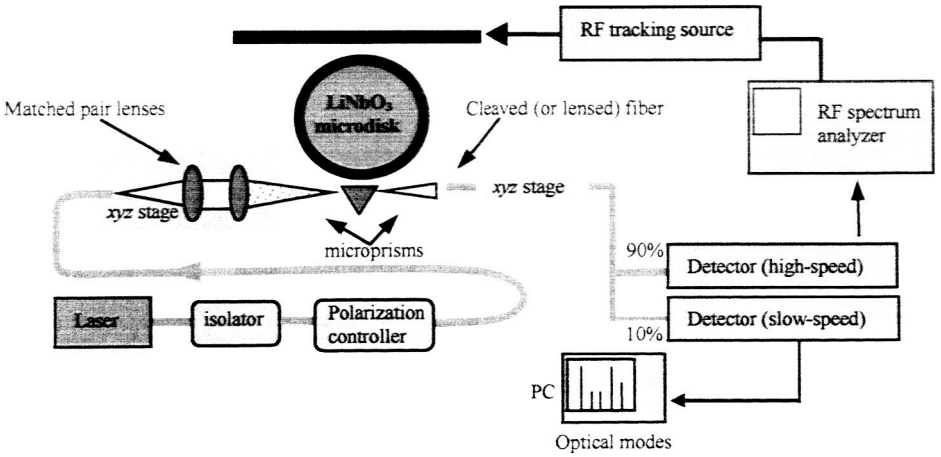

(b)

Figure 11 (a) Photograph of the Ku-band microdisk modulator. (b) Schematic diagram of the experimental arrangement used for evaluating the optical modulation performance of the microdisk modulator at single frequency.

The $LiNbO_3$ microdisk used in this arrangement is the same as Fig. 5(a) and 9(b) (400 μm thick, 3 mm in diameter with an optical free spectral range of 14.55 GHz). The copper ring resonator

has an outer diameter of 3 mm and width of 300 μm. The RF energy stored in the ring at resonance (f_{RF} = 14.55 GHz) is maximized by tuning the gap size (g). Fig. 12 shows the variation of the modulated optical power against peak-to-peak voltage of the input signal. The inset shows the modulated optical mode with a Q of 4×10^6. As may be seen at V_{pp} = 0.56 V the linear portion of the optical mode is completely modulated. Saturation of the linearly modulated optical power with increasing V_{pp} occurs because of increasing second-order harmonic generation due to nonlinear modulation. The optical intensity modulation is detected by a high-speed analog optical receiver with a responsivity of 260 μV/μW at 15 GHz. The calculated effective interacting voltage (based on DC shift and detector responsivity) is 3 V at −1 dBm (Vpp =0.56 V) RF input power that shows a voltage gain of 5.3 at resonance. The voltage gain calculated based on S-parameter measurements is 5.5. Fig. 12(b) shows the demodulated RF power against input RF power. The modulation saturation occurs around 0 dBm received RF power.

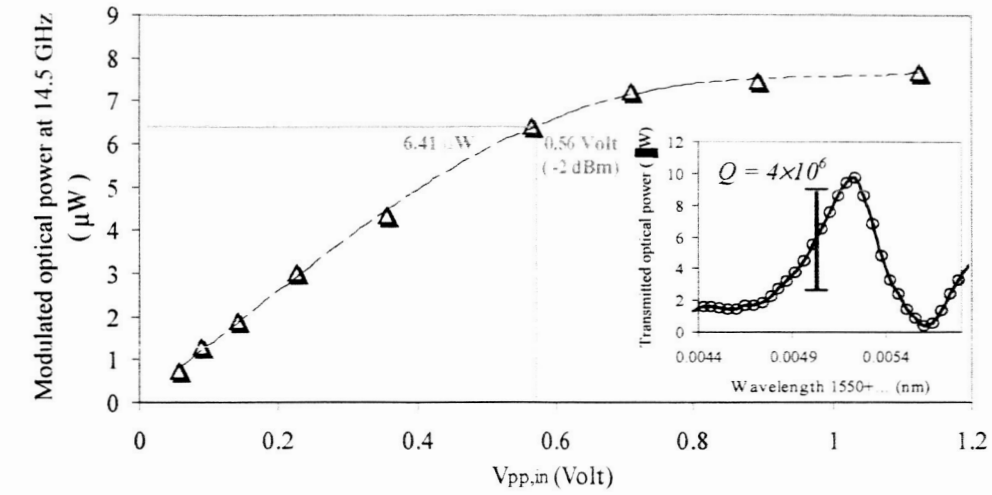

(a)

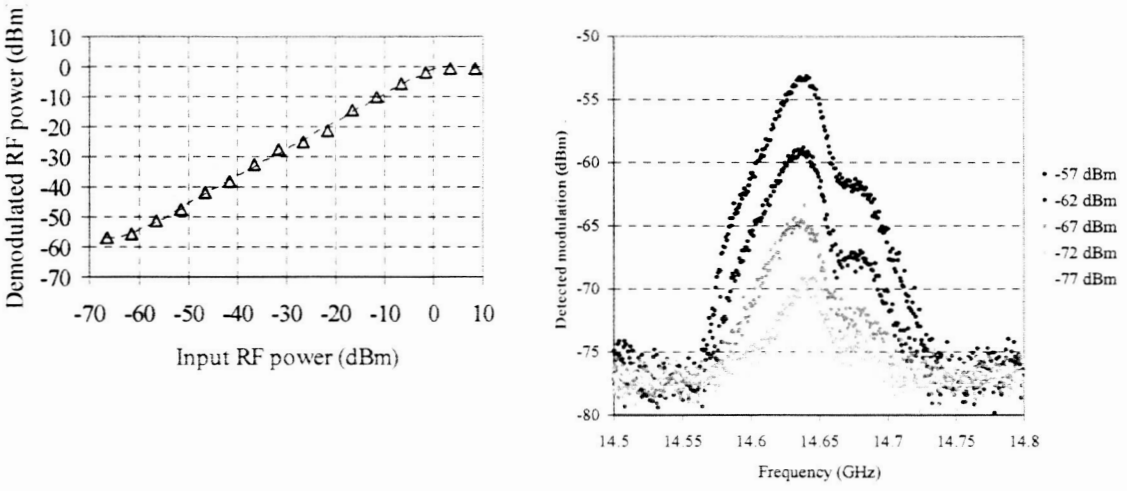

(b) (c)

Figure 12 (a) Linearly modulated optical intensity against peak-to-peak input voltage (and RF power). The inset shows the modulated optical mode. At V_{pp} = 0.56 Volt the optical power in the linear region of the optical mode is 100% modulated. (b) Demodulated RF power against input RF power. (c) Frequency spectrum of the detected RF power at very low RF input.

Fig. 12(c) shows the frequency spectrum of the detected RF power at very low RF input powers. In this experiment an RF amplifier with a gain of 20 dB is used after the detector to amplify the weak detected RF power. At -67 dBm received RF power the signal-to-noise ratio of the detected RF power is about 13 dB. Both saturation voltage and sensitivity measurement results shown in Fig. 12(b) and (c) show 10 dB improvement compared to the best results reported previously for a 9 GHz $LiNbO_3$ microdisk modulator [15].

If the modulating RF frequency (f_{RF}) is very close to $\Delta\nu_{FSR}$, the behavior of the microdisk modulator may be explained using a simple model based on the optical transfer function of the

microdisk optical resonator and electro-optic modulation of the WG *k*-vector. The time dependent extraordinary refractive index of the $LiNbO_3$ microdisk modulated by the voltage controlled by the ring resonator can be written as:

$$n_e'(t) = n_e + \delta n_e(t) = n_e + \frac{1}{2} n_e^3 r_{33} \frac{\beta_{EO}\beta_S}{h} \times G_v V_0 \cos(\omega_{RF} t)$$

where β_S (≈ 0.5) is a correction factor to compensate for the sinusoidal voltage distribution around the microdisk and V_0 is the amplitude of the input voltage Substituting n'_e in the optical transfer function one may estimate the modulated optical output power as a function of microdisk parameters. The modulated optical output power calculation may be simplified if we use the optical mode slope and the DC-shift as the main measurable parameters:

$P_{o,mod} = G_V \beta_S V_0 S \Delta\lambda_{DC}$

where $P_{o,mod}$ is the amplitude of the optical output power oscillation, and S is the optical mode slope in the vicinity of the laser wavelength (usually measured in μW/pm). This equation is valid only when the laser wavelength is tuned to the linear section of the optical resonance and $V_0 < (\Delta\lambda_{FWHM}/4\, G_V\, \Delta\lambda_{DC})$. These conditions guaranty the linearity of the modulation.

In an additional single frequency experiment with the 14.55 GHz microdisk modulator we selected a symmetric and clean WG resonance to estimate the voltage gain (G_V). The maximum mode slope (S) was 80 μW/pm. The RF input power was -1 dBm corresponding to a V_0 of 0.56 V. After correcting the modulated voltage and input RF power to compensate for the RF cable losses we calculated a G_V of 5.12 using the measured values of S, V_0 and $\Delta\lambda_{dc}$.

In section III we will show that if the laser wavelength is tuned to the resonant wavelength of a transmission dip or peak, the microdisk modulator can act as a square-law mixer. In the nonlinear modulation regime the sensitivity of the microdisk modulator is adequately quantified by the voltage amplitude that modulates half of the maximum optical output power. We call this voltage half-max-modulation voltage or V_{HMM} . Fig 13(a) shows the definition of V_{HMM} for a resonant transmission dip. Since V_{HMM} is the voltage amplitude of the RF input signal the voltage gain (G_v) is included in it. This is different than the earlier definitions based on DC response in the absence of the RF resonance. V_{HMM} is determined by the optical Q, h, r_{33}, and G_v. Fig. 13(b),(c) and (d) show the simulated values of V_{HMM} as a function of quality factor (Q), voltage gain (G_v) and microdisk thickness (h).

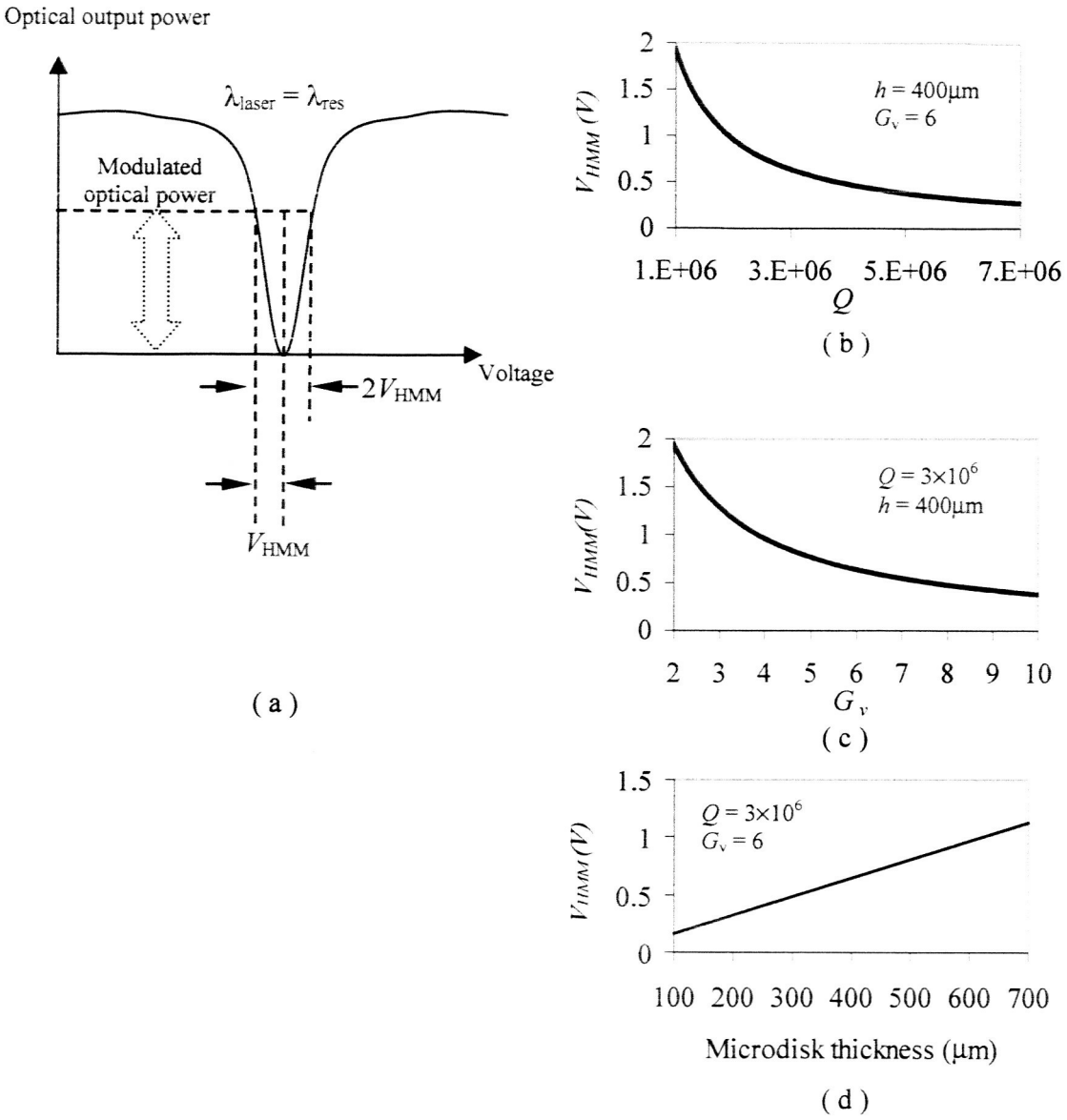

Figure 13 (a) Definition of V_{HMM} for a transmission dip. (b), (c) and (d) simulated values of V_{HMM} as a function of G_v ,Q and h using the electro-optic transfer function (f_{EO}).

Harmonic single frequency modulation

We have demonstrated efficient second-harmonic ($m_o = 2$) optical modulation by tuning the even second-harmonic resonance ($m_R = 2$) of the ring resonator to $2 \times \Delta\nu_{FSR}$. Fig. 14(a) shows a photograph of the experimental arrangement. The disk used is z-cut $LiNbO_3$ of diameter $D = 5.8$ mm and thickness $h = 0.720$ mm. Optical coupling into and out of the microdisk is achieved using a single microprism and the maximum coupled power is 100 μW. The optical Q is near 3×10^6 and $\Delta\nu_{FSR} \approx 7.6$ GHz (for TE WG modes). In this experiment first we compared the fundamental ($f_{RF} = \Delta\nu_{FSR}$) linear modulation efficiency of the ring and semi-ring resonator. Semi-ring resonator was previously used in the microdisk modulator design because its resonant frequency can be tuned simply by tuning the length [15,31,32,35].

Fig. 14(b) shows the measured S_{21} for the ring in Fig. 14(a) as well as a semi-ring on the same microdisk. The resonant dips up to the third harmonic of the ring are shown. For the ring resonator (solid line) we observe two dips (one small and one large) due to even-odd mode splitting.

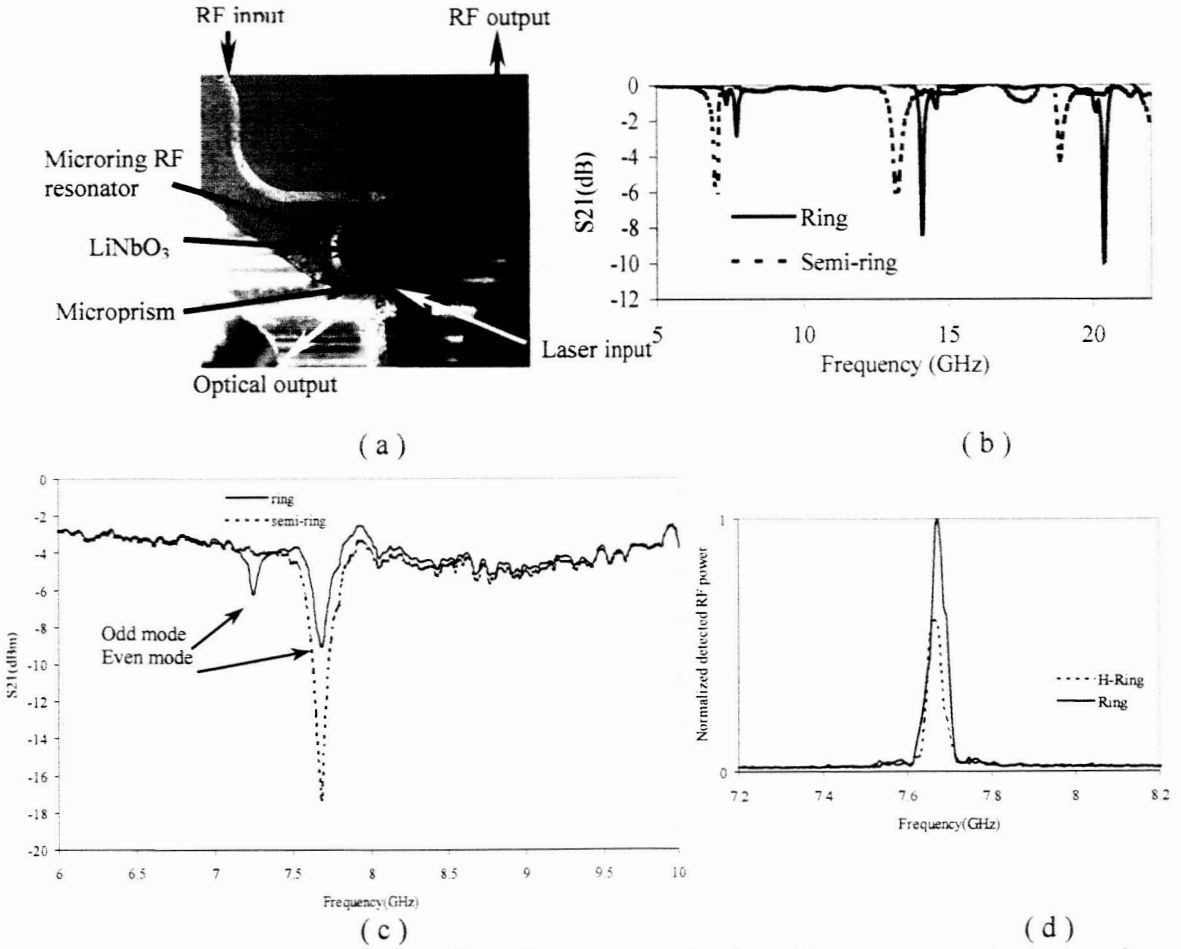

Figure 14 (a) Photograph of the experimental arrangement showing side-coupled microring, microprism, microdisk and output fiber. (b) S_{21} RF spectrum of a ring and semi-ring side-coupled to microstrip line. The copper microring has radius $R = 2.9$ mm and width $w = 0.5$ mm. (c) Measured S_{21} for semi-ring and ring at fundamental resonance. (d) The detected modulated power with semi-ring and ring resonator.

The coupling strength of the ring (depth of the resonant dips) at higher frequencies is better than that of the semi-ring and also the width of the resonant dips is smaller for the ring due to a better quality factor. These observations prove the superiority of the ring resonator especially at high frequencies. Fig.14(c) shows the measured S_{21} through the microstripline that is coupled to ring and semi-ring around the fundamental resonance. As may be seen the even mode of the ring and the fundamental resonance of the semi-ring are tuned to $\Delta\nu_{FSR}$. Fig. 14(d) shows the detected RF power from the detector showing modulation improvement replacing semi-ring with ring. Fig.15(a) shows a 3D view of the simulated *E*-field distribution for even second-harmonic mode on the ring (Because of *E*-field distribution and better coupling, we use the even modes of the ring modulation).

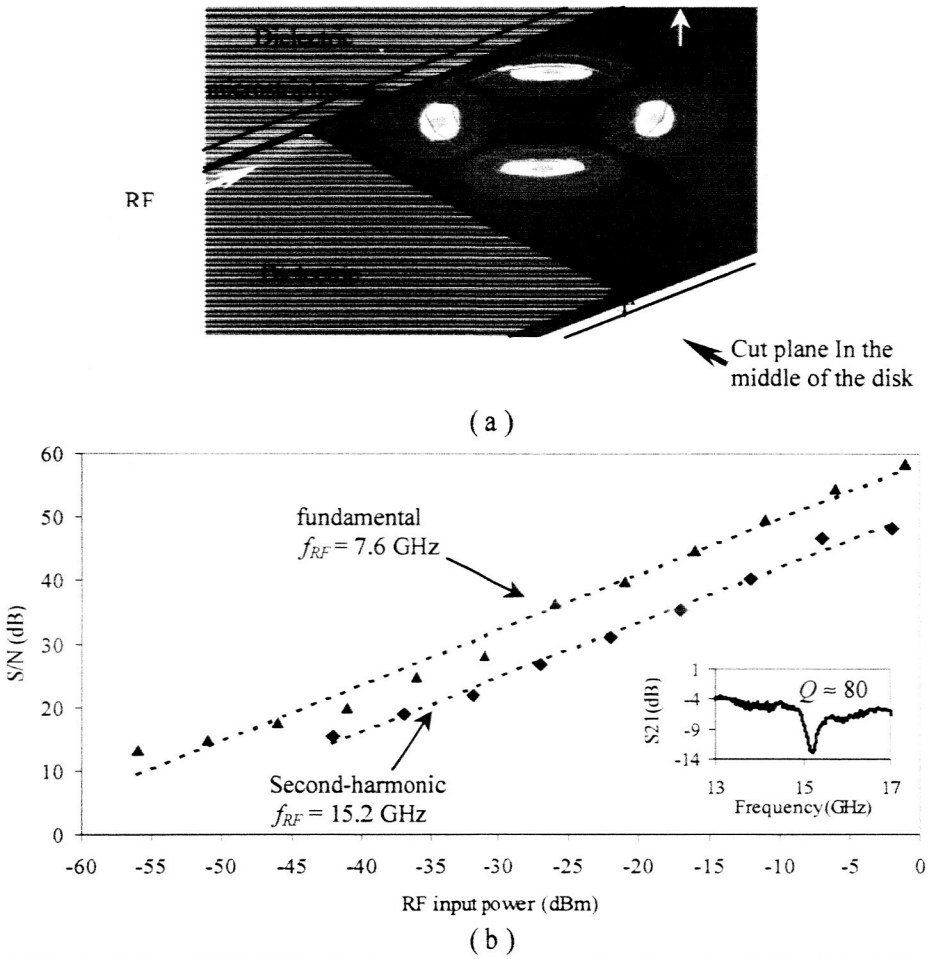

Figure 15 (a) 3D simulation of *E*-field distribution on a cut plane passing through middle of the disk when the even second-harmonic of the ring is excited. The plus signs correspond to *E*-vector directed upward along *c*-axis and minus signs correspond to downward direction. (b) Measured signal to noise ratio (of amplified signal) as a function of input *RF* power at fundamental (f_{RF} = 7.6 GHz) and second-harmonic (f_{RF} = 15.2 GHz) of the ring (the amplifiers have a gain of 30dB and noise figure of 1.7 dB and 2.6 dB respectively). The inset shows S_{21}spectrum when the even second harmonic of the ring (f = 15.2 GHz) is excited.

The plus sign means the *E*-vector is directed upward (along the c-axis) and minus sign means *E*-vector is pointing downward. Based on the *E*-vector directions it can be seen that the period of

RF oscillation is half the photon round trip time ($f_{RF} = 2 \times \nu_{FSR}$) the optical field stays in phase with the *RF*-field. Fig. 15(b) is measured signal to noise ratio (*SNR*) at the fundamental (ν_{FSR} = 7.6 GHz) and the second-harmonic ($2 \times \nu_{FSR}$ = 15.2 GHz). To have a bit error ratio (*BER*) performance of better than 10^{-7} (analog *SNR* of 20 dB) the minimum *RF* power needed is -32 dBm at 15.2 GHz and –41 dBm at 7.6 GHz. At ($f_{RF} = \Delta\nu_{FSR}$).

Fig. 16 shows the third-harmonic modulation results for the 8.7 GHz microdisk modulator. Fig. 16(a) shows the RF frequency spectrum of the detected third harmonic modulation ($3\times\Delta\nu_{FSR}$ = 3× 8.7 GHz = 26.1 GHz).

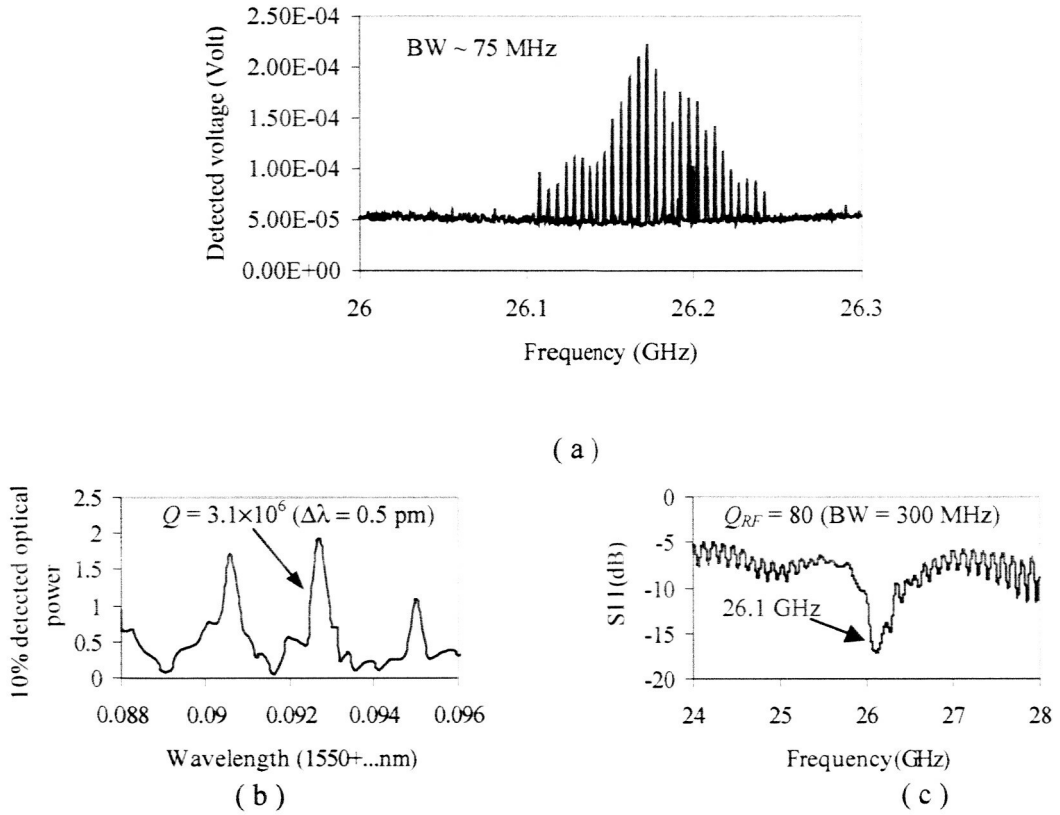

Figure 16 (a) RF frequency spectrum of the detected third harmonic modulation ($3\times\Delta\nu_{FSR}$ = 3× 8.7 GHz = 26.1 GHz). (b) The spectrum of the modulated optical mode. (c) S_{21} measurement result showing the 3rd resonance of the ring.

Fig. 16(b) shows the spectrum of the modulated optical mode with a Q of 3.1×10^6. The S_{21} spectrum result in Fig. 16(c) shows that the 3rd resonance of the ring resonator is tuned to $3\times\Delta\nu_{FSR}$.

Part II:

$LiNbO_3$ microdisk modulator in RF – optical link

The quality of the optical modulation in a $LiNbO_3$ microdisk modulator may be evaluated in an RF-optic link. We have demonstrated data and video transmission over a RF-optical link using a traveling-wave $LiNbO_3$ microdisk to modulate an optical carrier with a RF signal. Fig. 17(a) is a photograph of the side-coupled resonant modulator used in the experiments and Fig. 17(b) is a schematic diagram of the RF fiber-optic link.

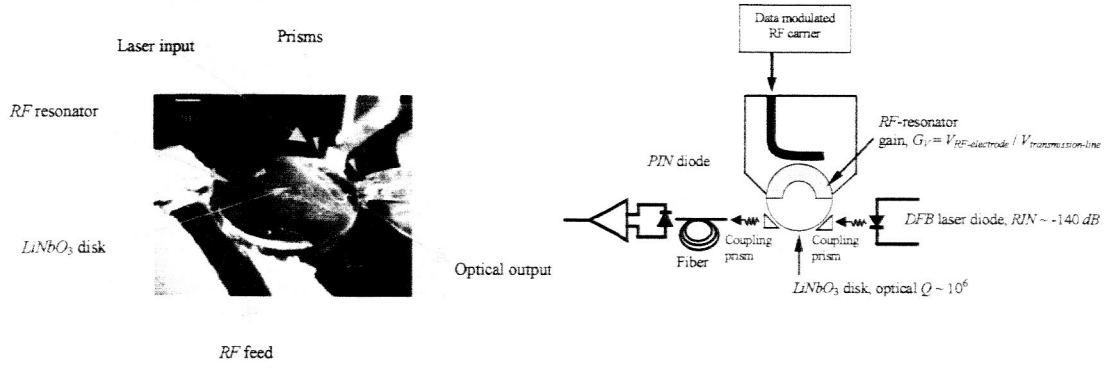

(a) (b)

Figure 17 (a) Photograph of the side-coupled resonant traveling-wave $LiNbO_3$ microdisk used to modulate an optical carrier with a *RF* signal. (b) Schematic diagram of the *RF* fiber-optic link used in the experiments.

The disk employed is z-cut $LiNbO_3$ of radius $R = 2.56$ mm and thickness $h = 0.4$ mm. A micro-prism couples laser light into the microdisk and another prism is used to couple light out. All components are mounted on a planar structure to improve mechanical stability of the system. The RF-resonator is a semi-ring metal electrode side-coupled to a microstrip line. The fundamental resonant frequency of the RF-resonator is tuned to match the 8.68 GHz optical free-spectral-range (FSR) of the disk so that simultaneous RF and optical resonance maximizes the electro-optic interaction. A RF synthesizer generates the RF carrier (at the first resonant frequency of the half-ring) that is modulated by a non-return-to-zero pseudo-random bit-stream (NRZ 2^7-1 PRBS) using a RF mixer. The resulting RF signal is then amplified and fed to the side-coupled ring resonator electrode used to modulate the 194 THz (wavelength $\lambda = 1550$ nm) optical carrier. After transmission through several meters of fiber, a PIN diode is used to detect and optical signal. The baseband data is down-converted through mixing with the local oscillator in a RF-mixer. The demodulated data is measured using a bit error ratio (BER) tester and a digital oscilloscope. The laser wavelength is tuned close to the resonant wavelength of one of the high-Q TE-modes of the disk where optical modulation is maximized. The bandwidth of the chosen optical-mode is about 150 MHz, corresponding to an optical $Q = 1.3 \times 10^6$, and this limits the data transmission rate to less than 200 Mb/s. The modulating RF power is the measured power of the RF signal (data modulated RF carrier) within 150 MHz bandwidth centered at 8.68 GHz RF-carrier frequency.

Fig. 18(a) shows the measured phase margin of the output at 10 Mb/s (NRZ 2^7-1 PRBS) for two different modulating RF-powers, 10 mW and 2.5 mW (2 and 1 Volt equivalent 50 ohm

terminated peak-to-peak voltage). The inset is a representative of the corresponding output eye-diagram.

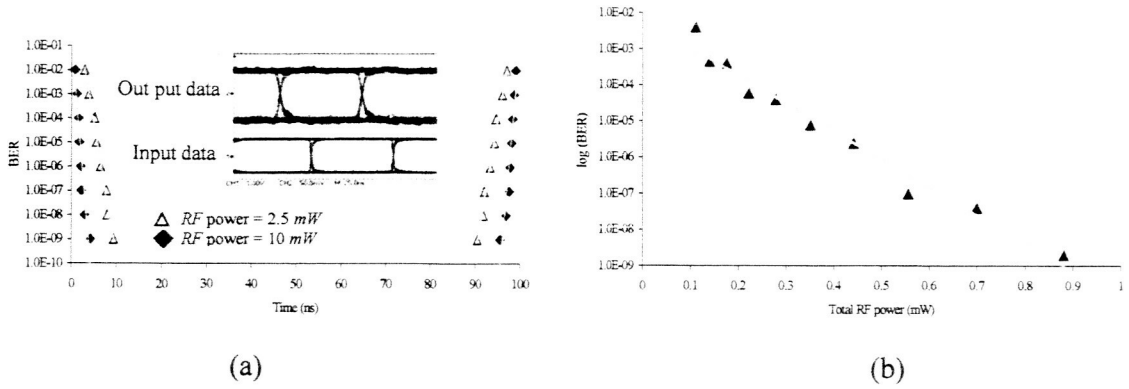

(a) (b)

Figure 18 (a) Measured phase margin of the output at 10 *Mb/s* (*NRZ* 2^7-1 *PRBS*) for 10 *mW* and 2.5 *mW* modulating *RF* power (the equivalent 50 ohm terminated peak-to-peak voltage (V_{pp}) is 2 and 1 Volt respectively). The inset is a representative of the corresponding output eye diagram. (b) Measured sensitivity of *BER* to modulating *RF* power (measured *RF* power within 150 MHz bandwidth centered at 8.68 GHz).

Fig. 18(b) shows the measured sensitivity of BER to modulating RF power. The optical output power for all of these measurements is between 18 μW to 27 μW and the laser wavelength is tuned close to the middle of the optical mode slope. Fig. 19 shows input and demodulated output eye-diagrams transmitted over the RF fiber-optic link at (a) 50 Mb/s and (b) 100 Mb/s NRZ 2^7-1 PRBS data rates.

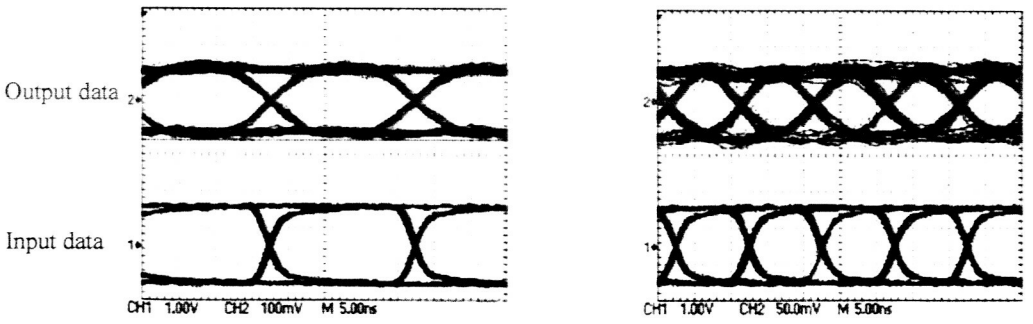

50 *Mb/s* (a) 100 *Mb/s* (b)

Figure 19 Input and demodulated output eye-diagrams transmitted over the *RF* fiber-optic link at (a) 50 Mb/s and (b) 100 Mb/s *NRZ* 2^7-1 *PRBS* data rates. The modulating *RF* power is 40 mW and 60 mW respectively.

The critical factors for high-quality data transmission are the purity and *Q*-factor of the chosen optical mode, the magnitude of the rising or falling slope of the optical mode in the vicinity of the laser wavelength, and the optical output power from the disk. By tuning the laser wavelength and RF carrier frequency it is possible to optimize the modulation quality and efficiency. Because of the high-*Q* of the optical modes (1 - 3 $\times 10^6$), the sensitivity of modulation quality and

efficiency to the mode's slope, wavelength stability of the laser is also important. A stable, high-quality, data transmission requires a wavelength stability of less than 0.1 pm.

To gain insight into the variables which most influence signal-to-noise and hence ultimate performance of the microdisk modulator for RF wireless applications we have investigated the sensitivity and BER performance of the modulator using realistic values of critical parameters. Contributions to signal-to-noise come from many sources these include laser relative intensity noise (*RIN*)aser line-width, optical detector dark current, detector amplifier noise, antenna background noise, etc. We found that laser *RIN*, microdisk optical *Q*, and *RF* electrode gain factor G_V are the important parameters determining sensitivity. Optical disk thickness, *h*, is also an important factor because, in the geometry we use, RF electric field intensity is proportional to *h*. Fig. 20(a) illustrates the sensitivity of the receiver to variation in optical *Q*. Increasing optical *Q* by a factor of two from 2×10^6 to 4×10^6 changes sensitivity by a factor of eight from 4.5 nW to 0.55 nW while decreasing the data bandwidth from 100 MHz to 50 MHz. Fig. 20(b) illustrates the sensitivity of the receiver to variation in microdisk thickness *h*. Decreasing t by a factor of two from 200 μm to 100 μm changes sensitivity by a factor of four from 2.5 nW to 0.66 nW. The improved value of sensitivity dramatically decreases BER so that values of BER in the 10^{-9} range can be achieved with RF input powers of less than 100 nW.

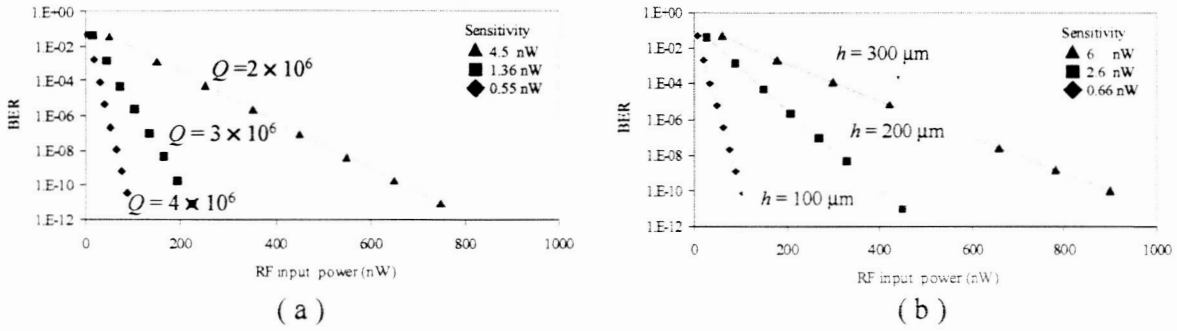

Figure 20 (a) Calculated sensitivity and *BER* as a function of *RF* input power assuming the indicated value of optical *Q*, optical coupling efficiency 15%, laser *RIN* of -150 dB/Hzisk thickness h = 400 μm, and RF Electrode voltage gain, G_V = 2. (b) Calculated sensitivity of *BER* as a function of *RF* input power assuming the indicated values of disk thickness *h*, an optical coupling efficiency of 15%, an optical *Q*-factor, $Q = 1.5 \times 10^6$, laser *RIN* of -150 dB/Hz, and *RF* electrode voltage gain, $G_V = 2$.

To achieve 10^{-9} BER with a few nW of received RF power requires simultaneous optimization of a few parameters. Fig. 17 shows the result of calculating sensitivity and BER as a function of RF input power assuming the indicated value of laser *RIN* and optical coupling efficiency. The device has thickness $h = 400$ μm, *Q*-factor is 2×10^6, RF electrode voltage gain $G_V = 10$. Notice, for the parameters simulated, optical coupling efficiency has little influence on BER with essentially the same results being obtained for 15% and 80% coupling efficiency for both curves. However, dramatically improved results occur when *RIN* is reduced from –140 dB/Hz to –150 dB/Hz. In the latter case, sensitivity is 50 pW and BER of 10^{-9} may be achieved at an RF input power of approximately 7 nW. These results are very encouraging and provide a systematic

approach with which to optimize for the microphotonic modulator to be used in the RF receiver. We anticipate our model will allow us to rapidly identify optimum modulator configurations.

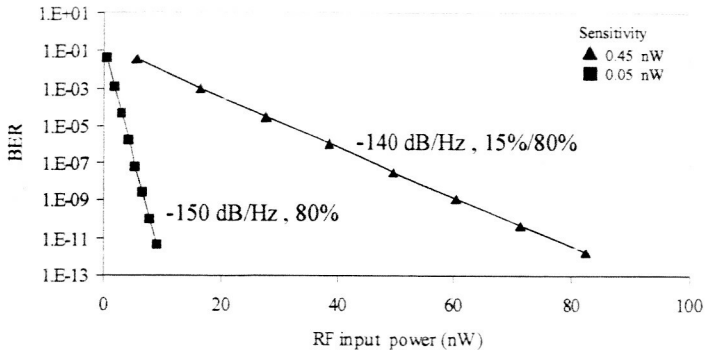

Figure 21 - Calculated sensitivity and *BER* as a function of *RF* input power assuming the indicated value of laser *RIN* and optical coupling efficiency. Disk thickness h= 400 μm, Q-factor is 2×10^6, *RF* electrode voltage gain G_V = 10.

Patch antenna and patch antenna arrays

Antennas for operation at 8, 15 and 30 GHz RF carrier frequency have been designed, fabricated to enable the demonstration of microdisk modulator performance in a wireless RF-optic link. We started working on planar antenna structures by design and fabrication of the single patch antenna at 8,15 and 30 GHz. In order to increase the radiated and detected power as well as improving the directionality of the radiation we switched to antenna patch arrays. Four-patch antenna array has been successfully designed and tested at 8 GHz and 14.5 GHz for application in two different microdisk optical receivers with 5.13 mm and 3 mm diameter disks respectively. Fig. 22(a) shows the photograph of the fabricated four-patch antenna array at 8 GHz and the definition of the coordinate system. The antenna has been fabricated on 0.5 mm thick duroid board with a permitivity of 2.94 and loss tangent of 0.00119. Fig. 22(b) shows the simulated radiation pattern of the antenna. As we see the radiation is effectively concentrated inside a 33° cone (3 dB angular width) in both H and E plane. Fig. 22(c) shows the experimental results of measuring the radiation patterns that are in good agreement with calculated results. The transmitting and receiving antennas were identical.

The same design has been scaled to 14.5 GHz and four-patch antenna array has been fabricated and successfully tested at 14.5 GHz. To increase the radiation power and make the radiation more directive we switched to a series-fed ten-patch antenna array.

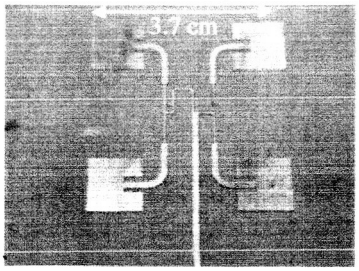

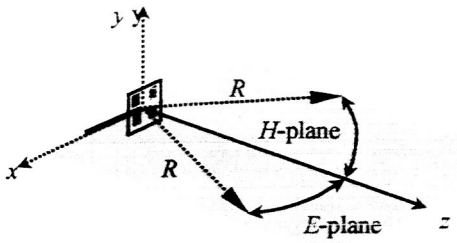

(a)

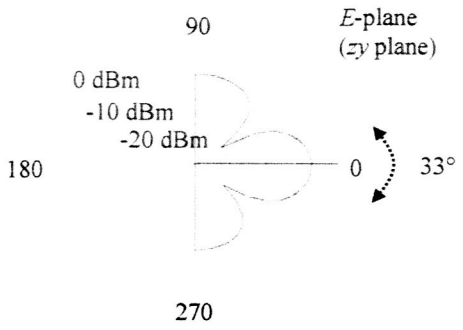

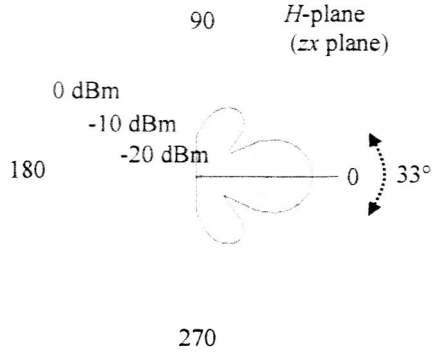

(b)

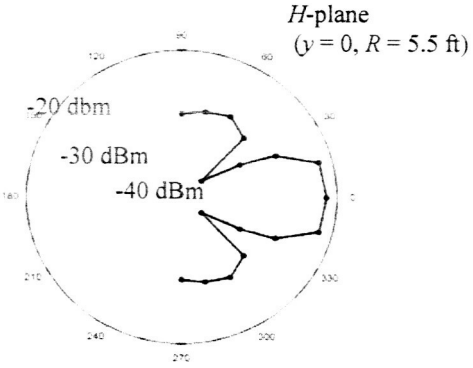

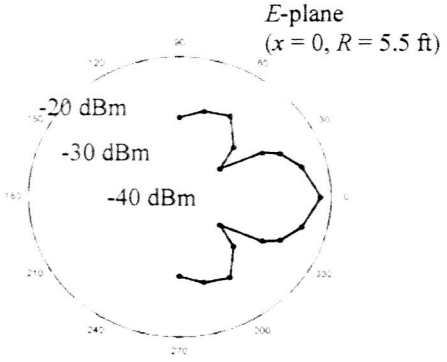

(c)

Figure 22 (a) Photograph of the fabricated 8.7 GHz four-patch antenna array and definition. (b) Definition of coordinates for characterizing the radiation pattern. (c) Calculated radiation pattern for antenna. (d) Experimental results of measuring the radiation pattern at 8.7 GHz.

Fig. 23(a) shows a photograph of the fabricated ten-patch series fed antenna array (on the same dielectric material) and the definition of the coordinate system. Fig. 23(b) shows the experimental results of measuring the radiation pattern as we see the vertical 3dB angular width (*E*-plane) decreased to 14°.

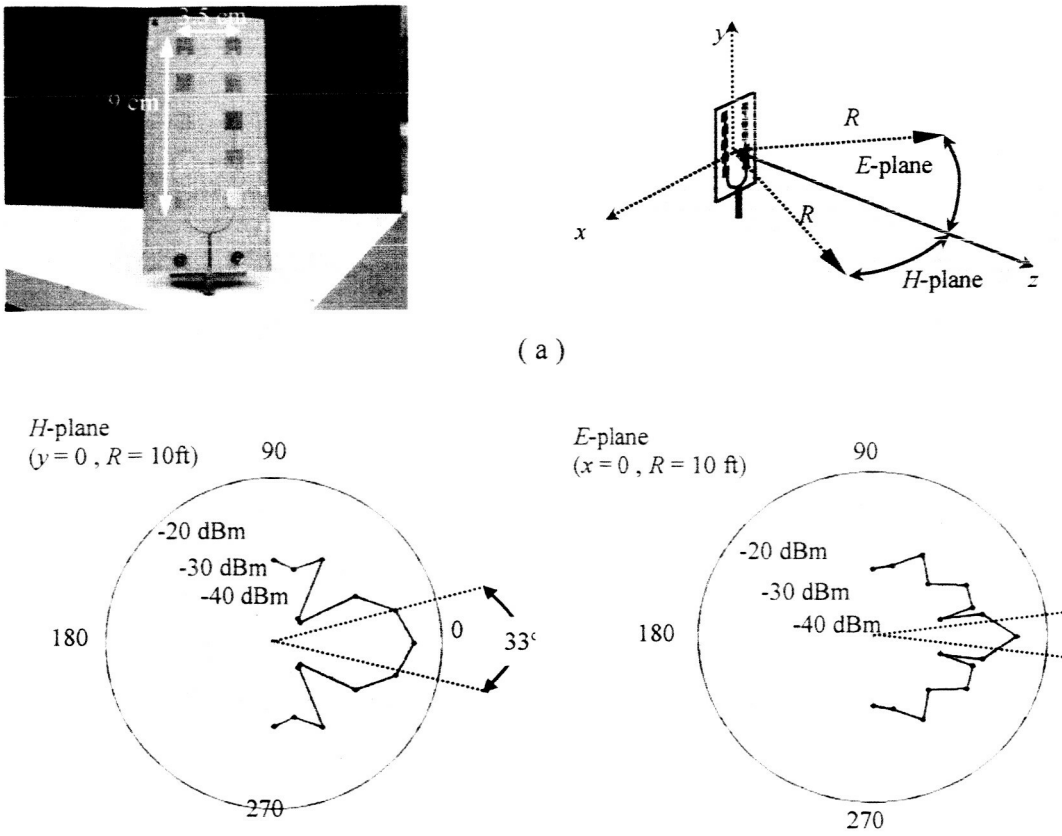

Figure 23 (a) Photograph of the fabricated 8.7 GHz series-fed ten-patch antenna array. (b) Definition of the coordinates for characterizing the radiation pattern. (c) Experimental results of measuring the radiation pattern at 8.7 GHz.

$LiNbO_3$ microdisk modulator in wireless RF – optical link

We have used the 4 and 10 patch antenna arrays designed for 8.7 GHz to demonstrate the performance of the microdisk modulator in a wireless RF-optical link. The antenna was directly attached to the microdisk modulator shown in Fig. 17. The transmitting antenna was a similar patch array fed by amplified data or video modulated 8.7 GHz carrier. We have successfully transmitted up to 100 Mb/s data stream and video signal over a 10 ft link. The operational distance of the link can be improved by employing more efficient antennas and more sensitive microdisk modulator.

Part III:

RF mixing/Down-conversion in optical domain

Processing microwave and mm-wave signals in the optical domain has been the subject of intensive research for the past few years [16-18]. Placing a RF signal on an optical carrier enables a wide variety of photonic signal processing techniques and, at the same time, avoids the use of lossy transmission lines and high-speed electronic devices. One of the key operations in microwave communication is frequency mixing. Several techniques have been proposed for RF mixing in the optical domain such as nonlinear modulation in a Mach-Zehnder modulator [19] and nonlinear detection in a photodiode [20]. Here we introduce a new photonic RF mixing technique that exploits simultaneous RF and optical resonance in the microdisk modulator. This is used to realize a photonic RF receiver without any high-speed electronic components.

In a conventional super-heterodyne RF receiver architecture a local oscillator (LO) and mixer are used to down-convert the signal to IF frequencies. Baseband information is subsequently extracted from the IF signal in a detector/demodulator. Alternatively, in a direct–conversion (homodyne) radio receiver, baseband information is obtained by mixing the received signal and the LO without using an IF frequency [21]. In addition to such approaches, self-heterodyne techniques have been proposed to reduce the number of components as well as size, weight, and power consumption in high-carrier frequency (mm-wave), short distance, applications [22]. In a self-heterodyne transmission system the transmitter broadcasts a RF modulated signal *and* the local carrier so the IF signal can be down-converted by mixing the received carrier and modulated signal in a nonlinear device called a self-mixer. The receiver power consumption, phase noise, and complexity are reduced as a result of eliminating the conventional LO and mixer. Although such an approach suffers from reduced power efficiency, it has been shown that it can lower overall cost and complexity in mm-wave local area networks and indoor wireless transmission systems.

Our photonic self-homodyne architecture combines direct-conversion, self-heterodyning, and microdisk modulator technology, to directly extract baseband information from the received signal by self-mixing of the transmitted carrier and the sidebands in the optical domain. We show that the second-order nonlinearity in the transfer function of a $LiNbO_3$ microdisk optical modulator when biased at its minimum transmission point may be used to realize the self-mixing process.

Microphotonic self-homodyne RF receiver

A photonic self-homodyne RF-receiver replaces the function of a single-ended diode or FET mixer in a transmitted carrier wireless link with a sensitive optical modulator that performs down-conversion in the optical domain. In this approach the nonlinear dependence of the modulator's transmitted optical power (P_{ot}) on applied RF voltage (V_{RF}) is the source of nonlinearity in the system. Fig. 24 illustrates the photonic self-homodyne RF receiver architecture. The received RF signal contains both sidebands and the center frequency (transmitted-carrier double-sideband modulation format) and is fed to an optical modulator

biased at its nonlinear operating point. The carrier and sidebands are mixed through the second-order nonlinearity ($P_{ot} \propto V_{RF}^2$), hence the optical output intensity spectrum contains the baseband and high-frequency products around the second-harmonic of the carrier frequency. A photoreceiver with a bandwidth matched to the baseband signal generates the baseband photocurrent (i_D) and automatically filters out the high-frequency components. The bandwidth of all electronic circuitry used in the system is no greater than that of the baseband signal.

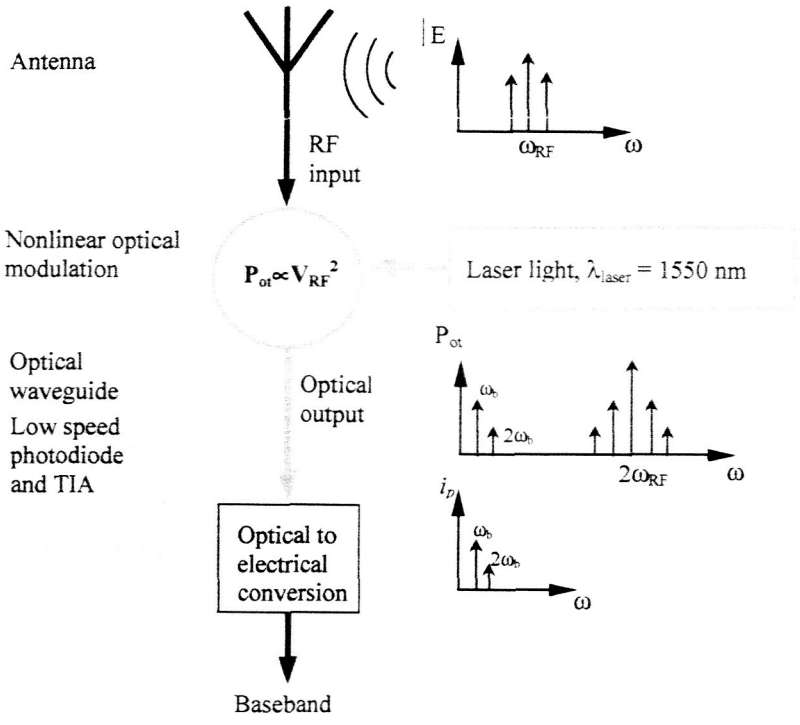

Figure 24 Schematic diagram of the photonic self-homodyne RF receiver. The transmitted carrier RF signal is received by the antenna and is directly fed to a square-law optical intensity modulator. Through nonlinear optical modulation the optical output intensity spectrum contains the baseband and high frequency components that are filtered out by the response of the low-speed photodetector.

The electro-optic transfer function of an optical intensity modulator $P_{ot}(V_{RF})$ can be expanded around $V_{RF} = 0$ to give:

$$P_{ot} = P_o^{(0)} + P_o^{(1)} + P_o^{(2)} + \ldots = N_0 + N_1 V_{RF} + \frac{N_2}{2} V_{RF}^2 + \ldots$$

Here, N_i ($i > 0$) is the ith Taylor expansion coefficient of $P_{ot}(V_{RF})$ at $V_{RF} = 0$ and N_0 is the transmitted optical power at $V_{RF} = 0$. At a fixed wavelength the magnitude of N_i depends on modulator properties and the chosen bias point. The first-order term linear optical intensity modulation ($P_{ot} \propto V_{RF}$) while other terms contribute nonlinear frequency components. Usually, such nonlinearities are minimized in conventional direct detection (DD) optical communication links. If the RF voltage amplitude is small enough and the modulator is biased at its extreme transmission point (where $dP_{ot}/dV_{RF} = 0$) the second-order term $P_o^{(2)}$ dominates the behavior of the modulator and the transmitted optical power (P_{ot}) dependence on voltage around $V_{RF} = 0$ will be similar to an ideal square-law mixer with:

$$P_{ot} \approx N_0 + \frac{N_2}{2} V_{RF}^2$$

If the baseband is a pure sinusoidal signal, the received RF voltage can be written as:

$$V_{RF} = V_0\left(1 + m_I \cos(\omega_b t)\right)\cos(\omega_{RF} t)$$

where m_I is the RF modulation index, ω_b is the baseband frequency and $\omega_{RF} = 2\pi f_{RF}$ is the RF carrier frequency. The second-order term can be written as

$$P_o^{(2)} = \frac{N_2}{2} \times V_{RF}^2 = \frac{N_2}{2} V_0^2 \left(1 + m_I \cos(\omega_b t)\right)^2 \cos^2(\omega_{RF} t)$$

Expanding the right-hand-side of this equation one obtains a DC term equal, high frequency components centered around $2\omega_{RF}$ and the two down-converted low-frequency terms at ω_b and $2\omega_b$ are given by

$$\frac{N_2 V_0^2 m_I^2}{8} \cos(2\omega_b t) + \frac{N_2 V_0^2}{2} m_I \cos(\omega_b t)$$

The total second-order modulated optical power is

$$P_{o,\max}^{(2)} = (1 + m_I^2 + 2m_I)\frac{N_2}{2} V_0^2$$

If we use a slow speed photodetector with a responsivity R, The optical power modulated at ω_b generates the baseband photocurrent i_b that carries the received information:

$$i_b = R\frac{N_2 V_0^2}{2} m_I \cos(\omega_b t)$$

The efficiency of this down-conversion process may be defined as the ratio between the amplitude of the optical power modulated at ω_b and $P_{o,max}^{(2)}$. This efficiency is limited by the generation of undesired frequency components at $2\omega_b$, $2\omega_{RF} \pm 2\omega_b$, and $2\omega_{RF} \pm \omega_b$ as well as the DC component. The linearity of the down-conversion is also an important parameter in receiver operation and is defined as the ratio of optical power modulated at ω_b and $2\omega_b$. Here we assume that the strength of the second-order nonlinearity dominates higher order so the generation of higher harmonics of the baseband ($3\omega_b$, $4\omega_b$, etc.) can be ignored. The down-conversion efficiency and its linearity are determined by the RF modulation index (m_I).

In Fig. 25 the down-conversion efficiency (a) and second-harmonic suppression ratio (b) are calculated against m_I. The second-harmonic baseband term ($2\omega_b$) can be suppressed relative to the baseband (ω_b) by employing a transmitted carrier RF modulation format ($m_I < 2$) and the down-conversion efficiency reaches its maximum value of 25% around $m_I = 1$. By choosing $m_I = 0.8$ an efficiency of about 25% and second-harmonic suppression of 7 dB optical (14 dB electrical, $P_e \propto i_p^2 \propto P_{ot}^{(2)}$) can be achieved. The sensitivity of a photonic RF receiver strongly depends on the magnitude of the second-order nonlinearity (N_2) and so is determined by the modulator sensitivity and the transfer function P_{ot}. Given that most wireless links only require a limited bandwidth around a high frequency carrier, a microdisk resonant optical modulator is a suitable choice for this application.

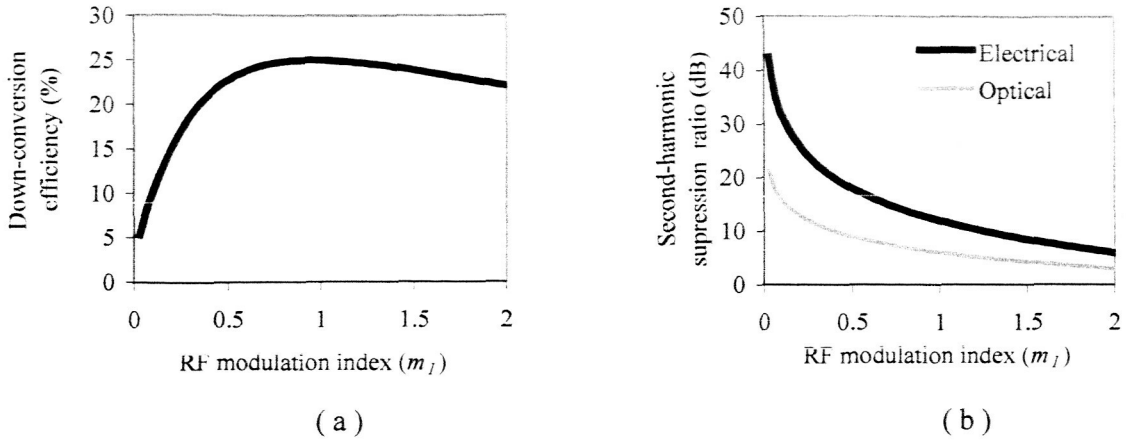

(a) (b)

Figure 25 (a) Calculated down-conversion efficiciency ($P_{o,\omega b}/P_{o,max}^{(2)}$) versus RF modulation index (m). (b) Second-harmonic suppression ratio against m. The electrical (after detection) and optical suppression ratios are related through $P_{e,\omega b}/P_{e,2\omega b}=(i_{\omega b}/i_{2\omega b})2\propto(P_{o,\omega b}/P_{o,\omega b})^2$

$LiNbO_3$ microdisk photonic RF mixer

At given RF voltage depending on the laser input wavelength the electro-optic transfer function of the microdisk modulator can have a linear or nonlinear functionality. Fig. 26 shows how the value of the laser wavelength relative to the resonant wavelength can change the linearity of the optical modulation in a microdisk modulator.

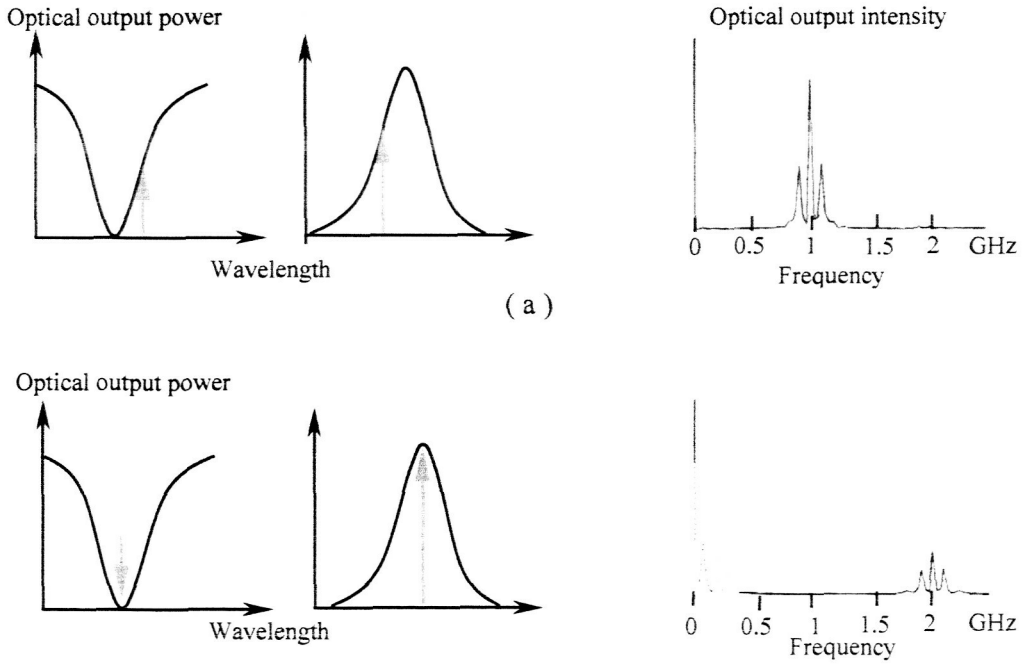

Figure 26 Simulated optical output power spectrum of microdisk modulator at linear (a) and nonlinear (b) operation regime. The RF input power is a 1 GHz RF carrier modulated by a 100 MHz (single frequency) baseband signal

Two cases has been simulated: (a) the laser wavelength is tuned to the middle of the mode slope where $P_{o,t} \propto V_{RF}$ (b) the laser wavelength is tuned to a resonant wavelength where $P_{o,t} \propto (V_{RF})^2$. The RF input voltage has the form $V_{RF} = V_o(1+m_i\cos(\omega_b t))\cos(\omega_{RF} t)$. The simulation clearly shows that when $\lambda_{laser} = \lambda_{res}$ the spectrum of the optical output power is similar to what is shown in Fig. 24. Fig. 27 illustrates the measured spectrum of the detected RF power when the microdisk modulator is fed by a single frequency RF signal ($V_{RF} = V_o \cos(2\pi f_{RF} t')$ $f_{RF} = \Delta\nu_{FSR} =$ 8.7 GHz). As may be seen when the laser wavelength is tuned to the resonant wavelength the linear modulated optical power (at 8.7 GHz) is suppressed and its second-harmonic (at 17.4 GHz) increases as a result of second-order nonlinear modulation or $P_{o,t} \propto (V_{RF})^2$.

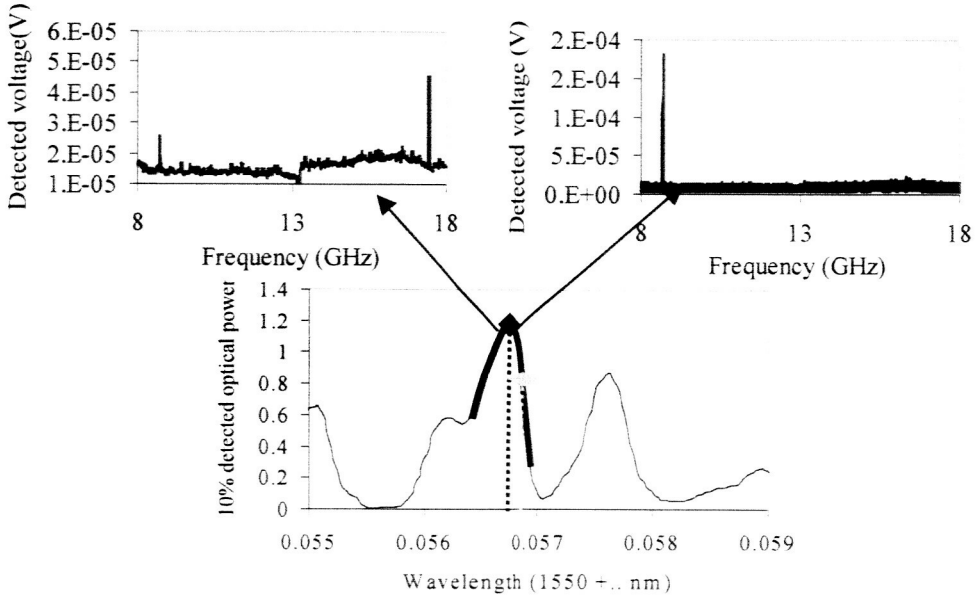

Figure 27 Nonlinear modulation with microdisk modulator. The microdisk is fed by a 0 dBm single frequency RF signal (f_{RF} = 8.7 GHz = optical free spectral range of the disk). When the laser wavelength is set to the middle of the optical mode slope the modulation is linear so we observe modulation only at 8.7 GHz (right) when the wavelength is at the peak, modulation becomes nonlinear and modulation occurs at 17.4 GHz while the linear component becomes small (left).

In the previous section we estimated the amplitude of the down-converted baseband modulated optical power for a general second-order nonlinear modulator. We showed that the baseband power is proportional to the second-order derivative of the electro-optic transfer function at a certain biased point (N_2). In Fig. 28 the transmitted optical power (P_{ot}) for a typical microdisk modulator is simulated as a function of input RF voltage (V_{RF}). In our simulation the modulator parameters are chosen to be representative of the experimental values with $Q = 3.5\times10^6$ (corresponding to $\alpha = 0.0075$ cm^{-1} and $\kappa_0 = 0.095$), $h = 400$ μm, and $G_v = 6$. The optical input power is 50 μW and $\lambda_{laser} \sim 1550$ nm. The laser wavelength is tuned to an optical resonance of the microdisk ($\lambda_{res} = \lambda_{laser}$) so in the absence of an external voltage ($V_{RF} = 0$) the transmitted optical power is minimized. At this bias point N_1 is zero and N_2 is maximized so the modulator

is operating in the extreme nonlinear regime. The sensitivity of the modulator can be quantified by a voltage amplitude V_{HMM} that modulates half of the optical mode power ($P_{o,mod} = P_{o,in} - P_{o,min}$). If $V_{RF} < 0.25V_{HMM}$ (small signal operating regime) the microdisk modulator is effectively operating as a square law optical intensity modulator ($N_i \sim 0$, $i > 2$) as explained in the previous section. Since the baseband modulated optical power is equal to $m_1N_2V_0^2/2$. N_2 is the critical parameter for down-conversion and is directly proportional to V_{HMM} and optical input power. Fig. 28 shows that V_{HMM} = 0.48 V and optical input power of 50 μW results in N_2 = 0.037 mW/V^2.

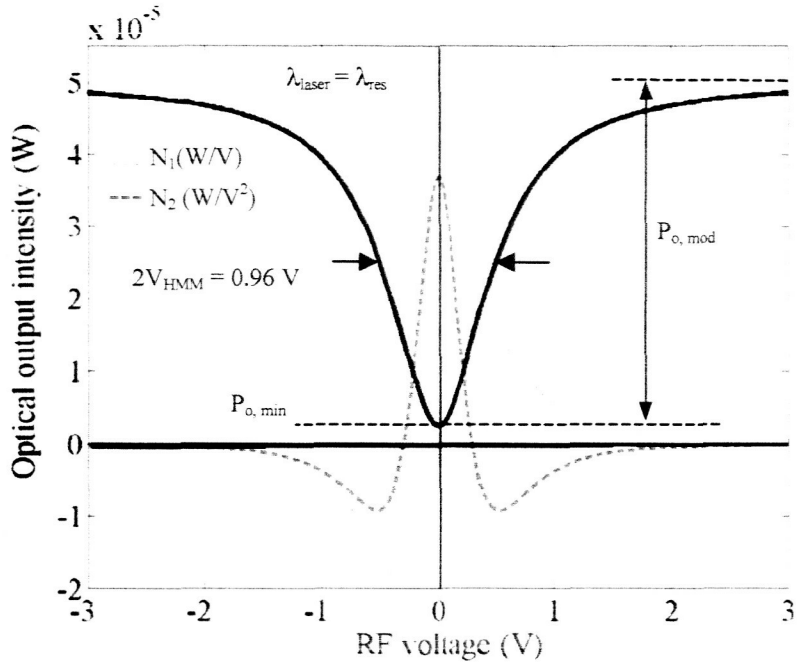

Figure 28 Calculated optical output intensity of an ideal microdisk modulator as function of RF input voltage (Gv = 6). The dashed and the dotted lines are generated as the first (N_1) and second (N_2) Taylor coefficients in an expansion of the optical transfer function (solid line). The laser is biased to the extreme nonlinear operating regime $\lambda_{laser} = \lambda_{res}$.

Both MZ modulator and microdisk modulator can be used for nonlinear optical modulation and RF mixing in optical domain. Fig. 29(a) and (b) shows the calculated optical output power against the applied RF voltage for a MZ and a microdisk modulator respectively (solid lines). The dashed curves are the parabolas defined by $(N_2/2)V^2$. At small signal regime (defined by the dotted boxes) where $V_{RF} < 0.25V_{HMM}$ ($< 0.25V_\pi$ for MZ modulator) the parabolas perfectly match the actual response, hence the strength of the second-order nonlinear modulation can be estimated simply by calculating N_2. So we can use the magnitude of N_2 to compare the performance of MZ and microdisk modulator as nonlinear modulators at small signal regime. The received RF signal for wireless communications is bellow –30 dBm corresponding to a voltage amplitude of less than 0.01 V. Knowing the typical value of V_{HMM} is between 0.2 V and 0.6 V and typical value of V_π is between 1 V and 5 V, our comparison is valid for all wireless applications. Fig. 29(c) shows the calculated value of N_2 versus V_{HMM} and V_π assuming the MZ has an insertion loss of 4 dB and microdisk modulator has an insertion loss of 10 dB. One may

see that the state-of-the-art $LiNbO_3$ MZ modulator with a V_π of 1 V has the same nonlinear modulation efficiency as a $LiNbO_3$ microdisk modulator with a V_{HMM} of about 0.4 V that can be easily made using a 200 μm $LiNbO_3$ thick microdisk.

More importantly the insertion loss of the microdisk modulator can be improved without affecting its sensitivity while in a MZ modulator generally enhanced sensitivity is accompanied by extra loss. So the 4 dB insertion loss for a MZ modulator with a V_π of 1 V is a very optimistic assumption while the 10 dB insertion loss and V_{HMM} of 0.5 V for a $LiNbO_3$ microdisk modulator is easily achievable by reducing the disk thickness to a 200 μm.

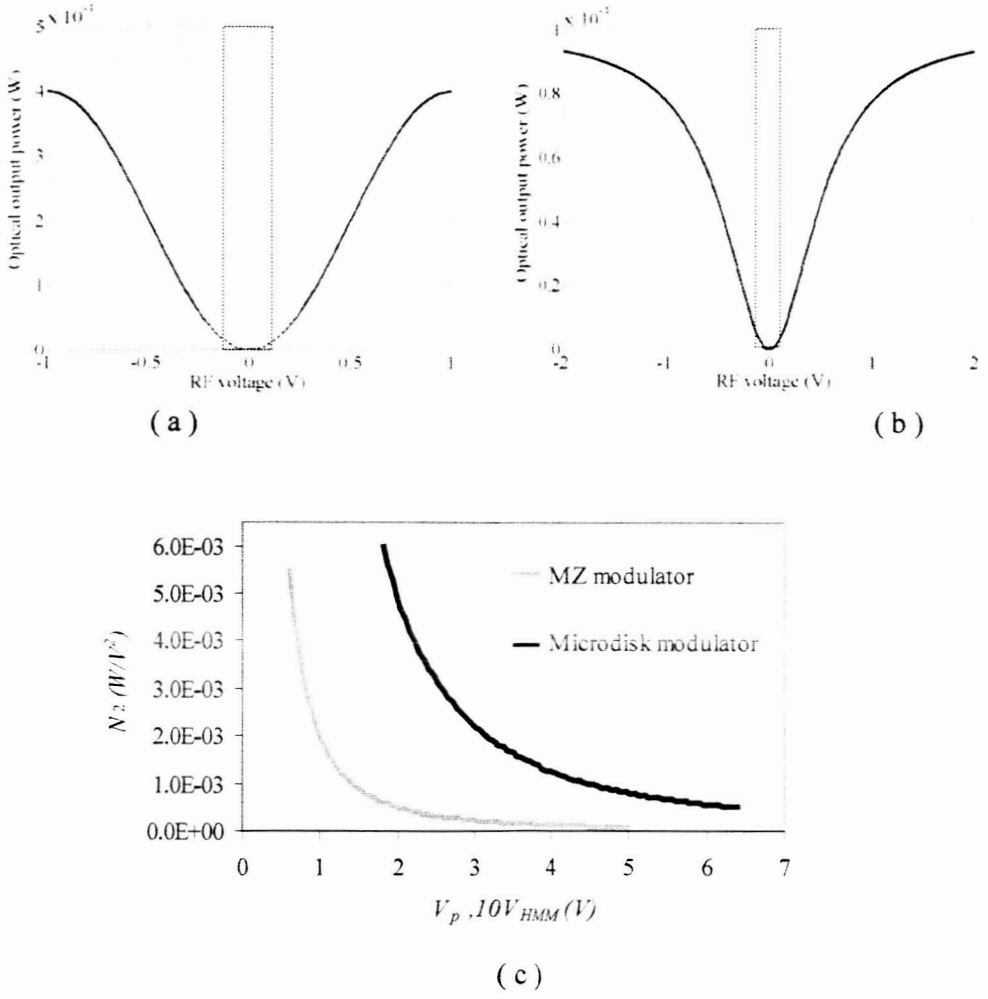

Figure 29 (a) Calculated optical output power against the RF voltage for a MZ modulator with a V_π of 1V and insertion loss of 4dB. The gray line is the approximated hyperbola $(N_2/2)V^2$. The dotted blocks shows the small signal region. (b) Calculated optical output power against RF voltage for a microdisk modulator with a V_{HMM} of 0.55 V and insertion loss of 10 dB. The optical input power is 1 mW. (c) Calculated values of N_2 versus V_{HMM} and V_π assuming the MZ has an insertion loss of 4 dB and microdisk modulator has an insertion loss of 10 dB

Although in most of our experiments the optical insertion loss was around 10 dB but insertion losses as low as 3 dB has been already demonstrated. Fig. 30 shows N_2 versus V_{HMM} for the $LiNbO_3$ microdisk modulator in Fig 30(b) and for three different values of insertion losses.

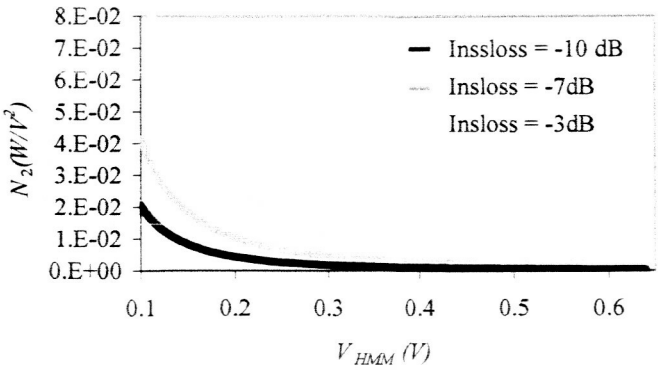

Figure 30 The simulated magnitude of N_2 as a function of V_{HMM} for different values of insertion loss. The optical input power is 1 mW.

Currently a commercial 10 GHz MZ modulator has a V_π of 4.5 V and an optical insertion loss of about 4 dB resulting in a N_2 of 9×10^{-5} W/V^2 at 1 mW optical input power. Our 14.6 GHz $LiNbO_3$ microdisk modulator has a V_{HMM} of 0.6 V and insertion loss of 10 dB. Resulting in a N_2 of 7×10^{-4} W/V^2 (at 1 mW optical input power) that is 8 times larger.

$LiNbO_3$ microdisk self-homodyne RF receiver

In our initial experiments we use a single tone baseband signal to study the effect of RF modulation index (m_I) and RF power on down-conversion efficiency and its linearity. Fig. 31(a) and (b) are the photographs of the 14.6 GHz microdisk modulator. Fig. 31(c) is a schematic diagram of the experimental arrangement. The modulator uses a 400 μm thick $LiNbO_3$ microdisk of 3 mm diameter and a free spectral range of $\Delta\nu_{FSR}$ = 14.6 GHz. The laser source is a tunable single mode laser with 0.05 pm wavelength resolution and a linewidth of less than 0.5 MHz. The laser wavelength is always tuned to the minimum of the chosen transmission dip to maximize the second-order nonlinear modulation strength (N_2). The RF signal is a 10 MHz single tone baseband signal mixed with a 14.6 GHz RF-carrier in a double-balanced RF-mixer. By DC-biasing the IF port of the mixer we can control the modulation index (m_I) and magnitude of the transmitted power at the carrier frequency. The RF signal is fed to the microdisk modulator through a bandpass RF filter with 1 GHz bandwidth around 14.5 GHz, to make sure that all of the nonlinear products generated in the RF components are filtered out. The optical output is detected in an amplified photodetector with a bandwidth of 150 MHz and responsivity of 3 mV/μW.

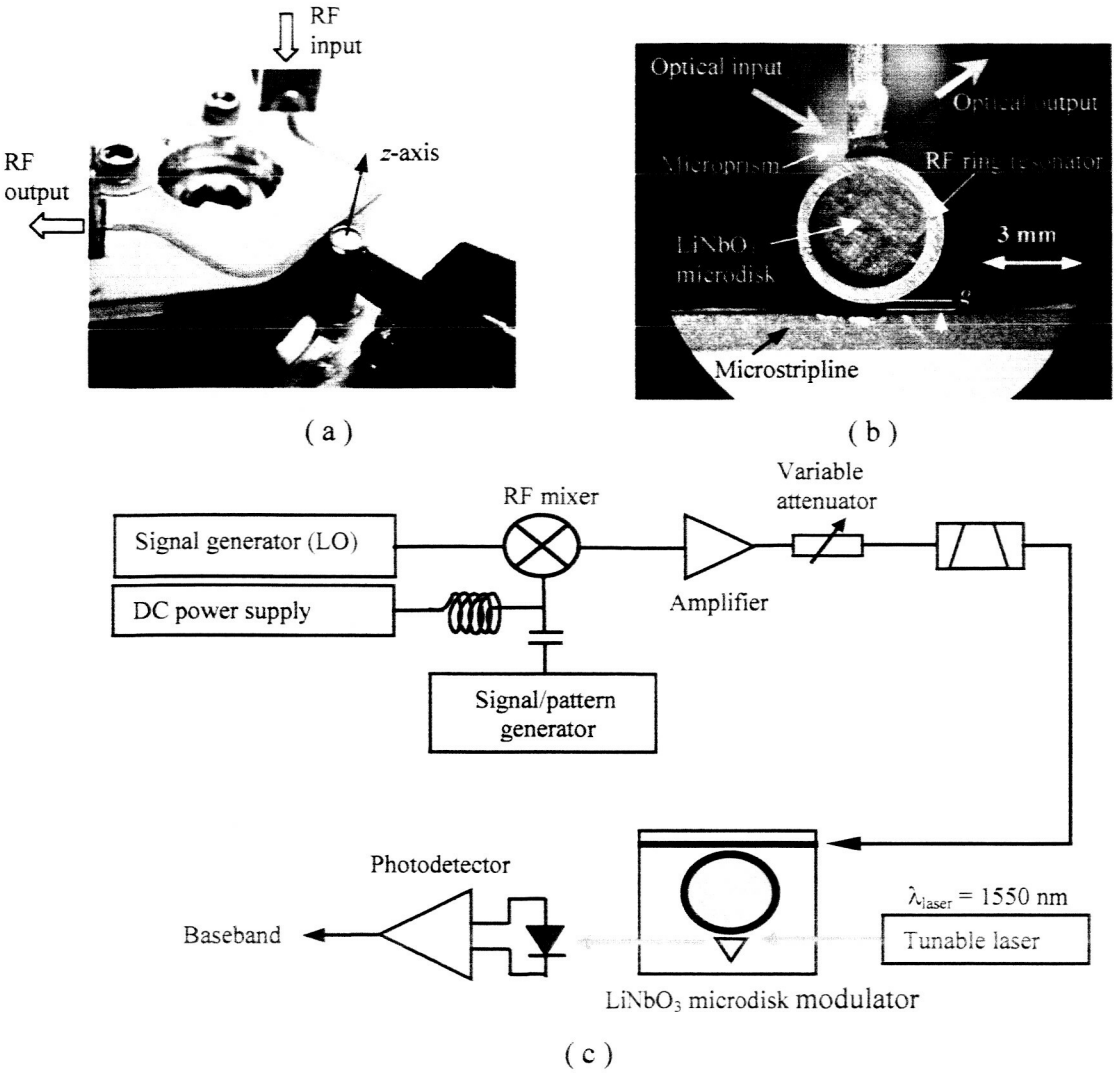

Figure 31 (a) Photograph of the $LiNbO_3$ microdisk modulator. (b) A close up view of the modulator showing the microstripline, $LiNbO_3$ microdisk, microprism, microring RF resonator and the output fiber. (c) Schematic diagram of the experimental arrangement used for photonic RF down-conversion measurements. The RF modulation index (m_I) is tuned using the DC bias on the mixer. The laser is a tunable single mode laser with a resolution of 0.1 pm and linewidth of less than 0.5 MHz. The RF filter eliminates any low frequency component generated due to nonlinearities in RF devices. The local oscillator frequency is 14.6 GHz that is equal to the optical free spectral range of the microdisk modulator.

Fig. 32 shows the down-converted optical power against the total RF input power when $m = 0.8$. The black circles are the experimental data and the white circles and dashed line are the simulated data. The inset shows the optical resonance selected for nonlinear modulation. The black arrow indicates the location of the laser wavelength, λ_{laser}. The optical resonance has $Q = 2.7\times10^6$ and a N_2 coefficient of 0.023 mW/V^2 ($V_{HMM} = 0.7$ V). The simulated data in Fig. 32 are calculated using $mN_2V_0^2/2$ and knowing that the total average RF power of a single tone. modulated RF carrier is given by $P_{RF} = V_0^2(1+m^2/2)/100$.

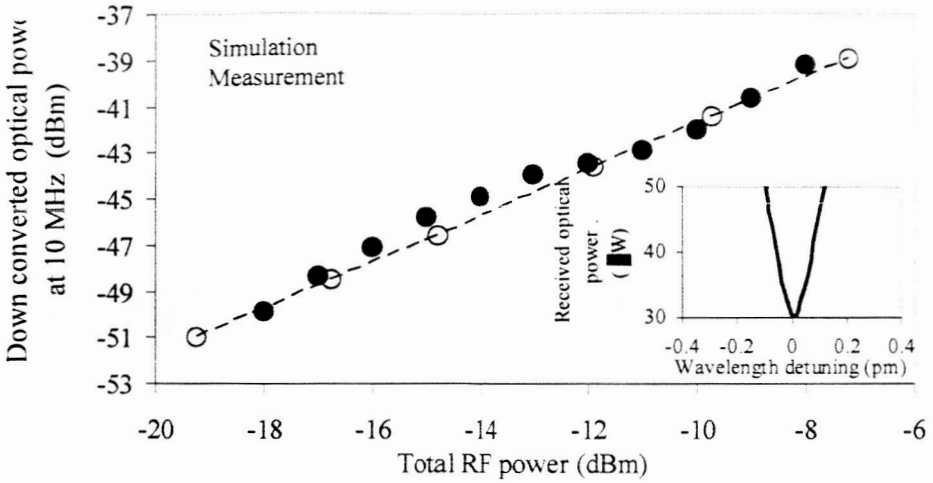

Figure 32 Measured baseband modulated (10 MHz) optical output power against m_I for three optical modes with different optical quality factors.

Fig. 27(a) shows the variation of the down-converted optical power at 10 MHz as a function of the modulation index m_I and for three resonances with different quality factors. The modulation index is tuned to the desired values by changing the DC bias applied to the mixer.

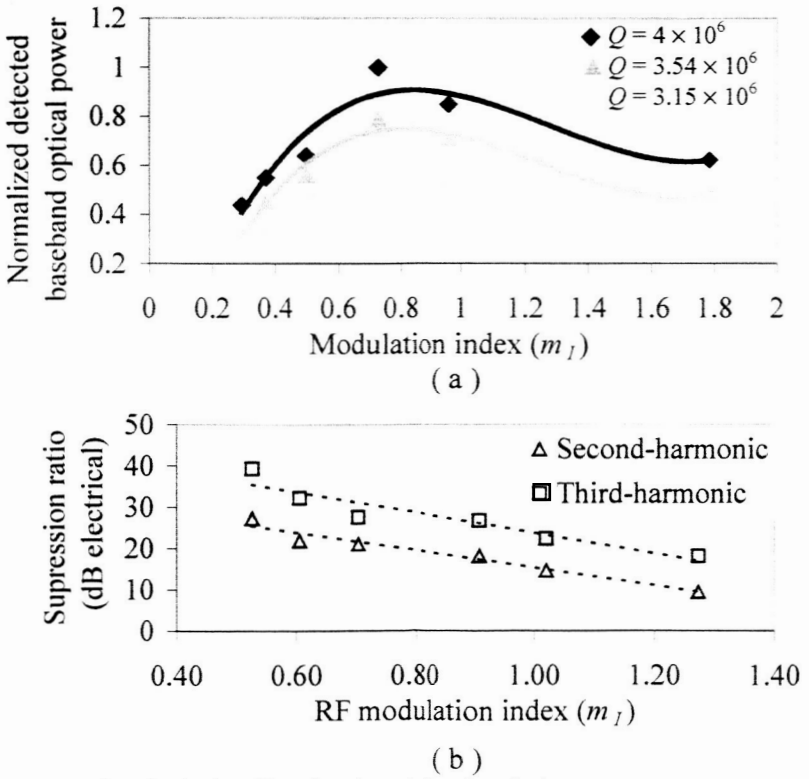

Figure 33 (a) The measured and calculated baseband modulated optical power versus total RF input power. The inset shows the optical spectrum of the WG resonance chosen for down-conversion (Q = 2.7×10^6, N_2 = 2.23×10^{-2} mW/V^2). (b) Measured second and third Harmonic suppression ratios (electrical) against m_I.

The total received RF power is about -15 dBm that corresponds to $V_0 = 0.05$ V (3). The V_{HMM} is around 0.8 V for the optical resonance used, so $V_0 < 0.25\ V_{HMM}$ guarantees device operation in the small-signal regime. As may be seen in Fig. 33(a), down-conversion efficiency is maximized around $m = 0.8$, in very good agreement with the simulated curve for an ideal square law mixer. Also, as anticipated, the amount of down-converted power increases as we increase the optical Q (a larger Q results in a larger V_{HMM} and therefore a larger N_2). To evaluate the linearity of the down-conversion process we have measured the detected power at the second and third harmonic of the baseband signal (20 MHz and 30 MHz respectively).

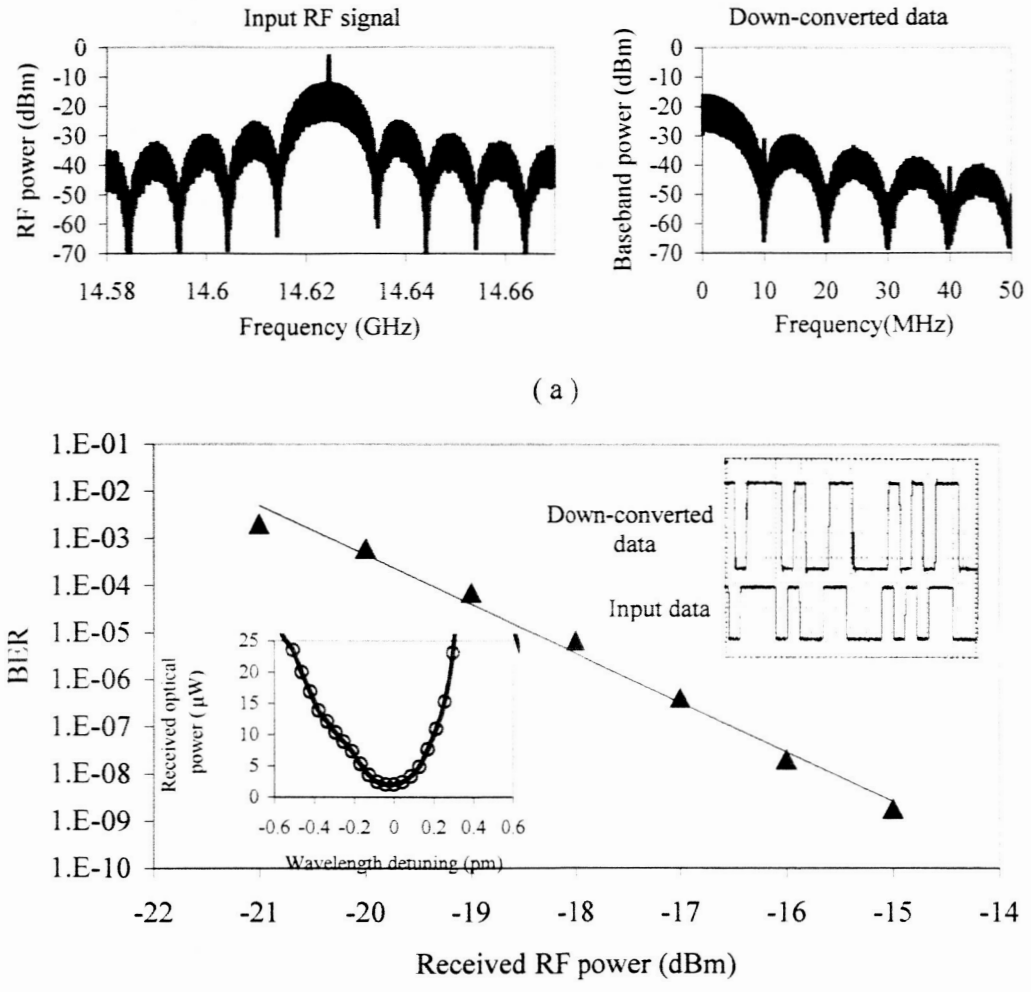

Figure 34 Measurement results of photonic data down-conversion in $LiNbO_3$ microdisk modulator. (a) The frequency spectrum of the input RF signal and down-converted signal. The RF carrier frequency is 14.6 GHz and it is modulated by a 10 Mb/s 2^7-1 NRZ PRBS bit stream. (b) The BER sensitivity of the photonic RF receiver. The RF power is the measured RF power within 10 MHz bandwidth centered around 14.6 GHz. The right inset shows the input and detected data in time domain. The left inset shows the optical spectrum of the selected WG resonance

In a perfect square law modulator the third harmonic should be absent but the chosen optical resonance doesn't have an ideal symmetric shape and so generates odd harmonics. Fig. 33(b) shows the harmonic suppression ratio against m_I. As predicted (Fig. 25(b)) the suppression ratio decreases when we increase m_I. At $m_I = 0.8$ the second-harmonic suppression ratio is about 17 dB (electrical).

For experimental demonstration of data transmission we use the arrangement in Fig. 31(c) but replace the signal generator with a NRZ pattern generator and the photodetector with a digital photoreceiver. The photoreceiver has a –3 dB frequency bandwidth of 120 MHz and a sensitivity of –34.5 dBm. Fig. 34(a) shows the measured frequency spectrum of the input RF signal and the down-converted signal after detection. The carrier frequency is 14.62 GHz and the baseband data is a 10 Mb/s NRZ 2^7-1 pseudo-random bit stream (PRBS). Fig. 34(b) shows the measured bit error ratio (BER) against the total RF input power. The received RF power is defined as the measured RF power within 10 MHz bandwidth centered around 14.6 GHz. The left inset shows the spectrum of the optical resonance with $Q = 2\times10^6$. The inset on the right shows the input and down-converted data in the time domain.

In Fig. 35 the measured eye diagrams at 10 Mb/s, 50 Mb/s and 100 Mb/s are shown. The received RF power is –15 dBm. In this particular case the maximum data rate is limited by the optical Q to approximately 100 Mb/s.

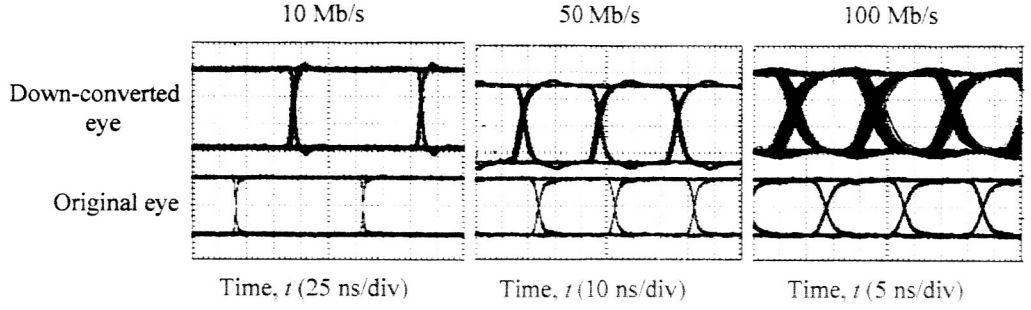

Figure 35 Measured eye diagrams at 10 Mb/s, 50 Mb/s and 100 Mb/s.

We note that the detected down-converted signal can be increased by reducing the disk thickness (h) and employing a high-Q RF ring resonator (both these factors lead to a larger N_2 coefficient). We can also reduce the signal-to-noise in the photonic receiver by employing a bandpass optical filter after the microdisk modulator. A filter with a bandwidth less than $4f_{RF}$ can eliminate high frequency optical components around $2f_{RF}$ given and therefore reduce the noise generated by the optical power at these frequencies in the slow-speed photoreceiver.

Wireless transmission using the photonic receiver

We have designed and fabricated a 4-patch antenna array with 1 GHz bandwidth around 14.6 GHz carrier frequency to demonstrate the first microphotonic RF wireless receiver in Ku-band. The antenna is directly attached to the microdisk modulator. In a one directional indoor wireless link the transmit antenna can have a fix position while the receive antenna moves in the area covered by the transmitted radiation. In this case, replacing the small 4-patch transmitting antenna with a high gain parabolic antenna may increase the link length. In our experiment we

use a parabolic antenna with a diameter of 1 ft, gain of 33 dB and 3 dB bandwidth of 110 MHz around 14.8 GHz. The beam width is about 3.5 degree.

Fig. 36(a) shows a schematic diagram of the wireless-photonic link. The transmitted carrier signal is amplified and then fed to the parabolic antenna through a bandpass filter. The amplifier has fix gain of 33 dB. The modulation format and the power of the RF signal are controlled by LO power and the DC bias on the mixer.

The receiving antenna (which is a 4-patch array) is located 45 ft apart from the transmitter and is directly attached to the microdisk modulator with a coaxial cable. Fig 36(b) shows the parabolic antenna used as the transmitter and Fig. 36(c) shows the microdisk photonic receiver (4-patch antenna array and the microdisk modulator). The 4-patch antenna has a gain $G_r = 10$ while the parabolic antenna has a gain of $G_t = 1900$. In our experiment the input RF power to the transmit antenna is 19 dBm and the received power is –20 dBm.

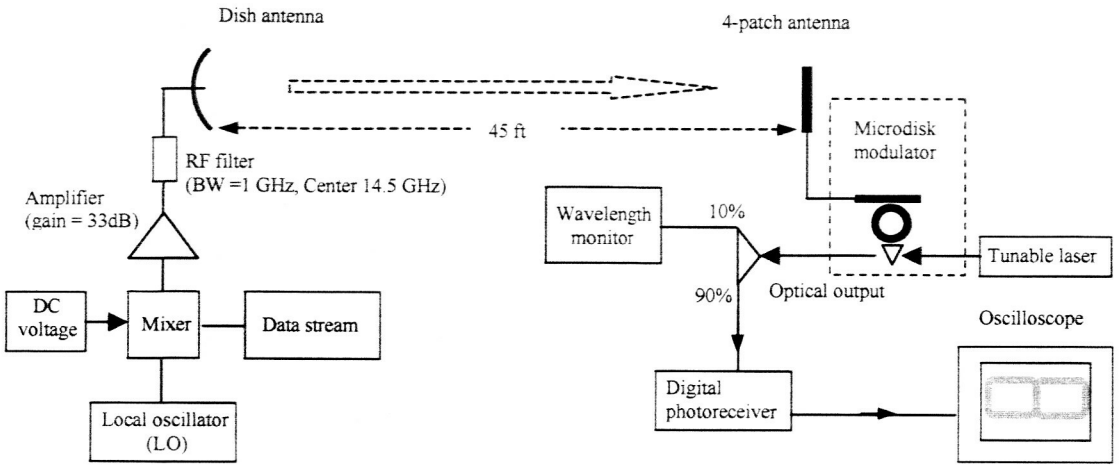

(a)

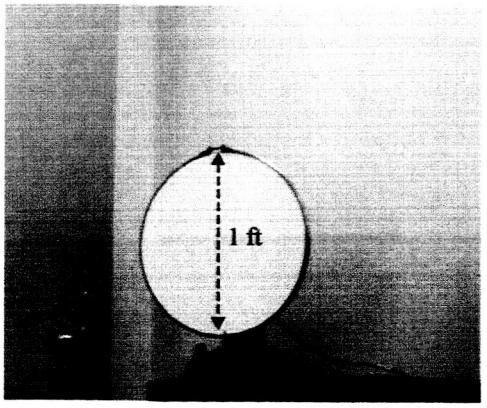

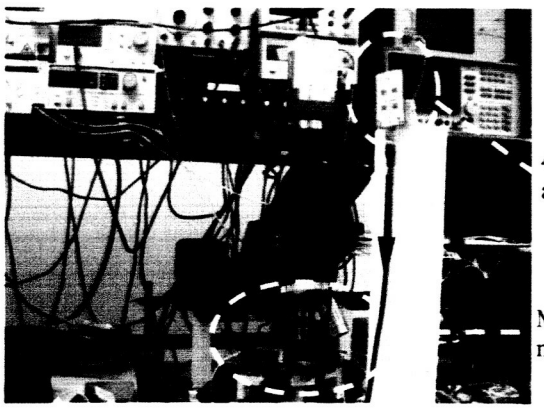

(b) (c)

Figure 36 (a) Indoor wireless link with a parabolic transmit antenna and microdisk photonic receiver. The signal is transmitted through a 45 ft long wireless link and the baseband information is down-converted in a microdisk photonic receiver. (b) The parabolic antenna used as the transmitter. The antenna has a diameter of 1 ft and a gain of 33 dB. (c) The microdisk photonic receiver: 4-patch antenna array and the microdisk modulator.

The measured value of the received RF power is in good agreement with the Friis formula: $P_r=P_tG_rG_t\lambda^2/(4\pi R)^2$, where P_r is the received power P_t is the input power to the transmit antenna, λ is the wavelength (2.1 cm) and R is the distance between two antennae (14 m).
Fig. 37(a) shows the spectrum of the optical resonance chosen for photonic down-conversion. The optical input power is 1 mW while the maximum transmitted optical power is about 30 μW this corresponds to an optical coupling efficiency of 3%. Fig. 37(b) shows the electro-optic transfer function of the optical resonance with a V_{HMM} of 0.6 Volt. The solid line is the estimated parabolic behavior at small signal regime. The second derivative (N_2) has a value of 0.0026 W/V^2. The digital photoreceiver has a sensitivity of –40 dBm (for a BER 0f 10^{-9}) and digital bandwidth of 52 Mb/s.

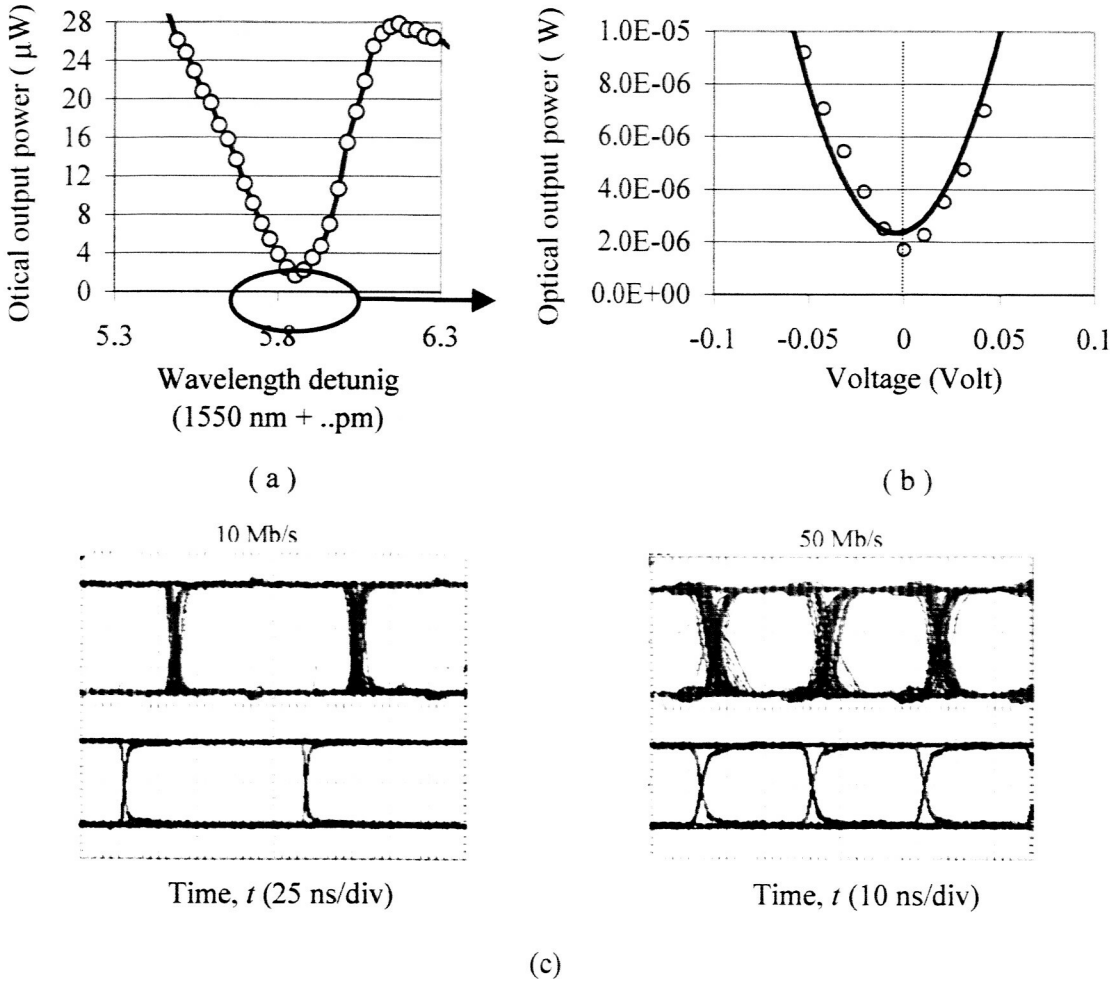

Figure 37. (a) The spectrum of the optical resonance chosen for photonic down-conversion. (b) The electro-optical response of the optical output power. The solid line is the estimated parabolic behavior at small signal regime. (c) Measured eye diagrams after photonic down-conversion from 14.6 GHz carrier. The data is NRZ 2^7-1 PRBS and the measured BER is 10^{-6} at –20 dBm received RF power for both 10 Mb/s and 50 Mb/s data streams.

Fig. 37(c) showes the measured eye diagrams after photonic down-conversion from 14.6 GHz carrier. The data is NRZ 2^7-1 PRBS and the measured BER is 10^{-6} at –20 dBm received RF power for both 10 Mb/s and 50 Mb/s data streams.

Part IV:

Sensitivity of microdisk photonic receiver

We have shown that the efficiency of down-conversion in a photonic mixer is directly proportional to the second derivative of the electro-optic transfer function (N_2). For a microdisk modulator N_2 is determined by the maximum optical output power ($P_{o,max}$) and V_{HMM}. Since $P_{o,max}$ = optical insertion loss × $P_{o,in}$, Optical insertion loss, optical input power and V_{HMM} are the determining factors for the down-conversion efficiency of the microdisk photonic mixer.
So the overall sensitivity of the self-homodyne microdisk receiver is a function of all of the above-mentioned parameters plus the sensitivity of the digital photoreceiver.

If the sensitivity of the digital photoreceiver and the wireless RF receiver are defined based on the same bit error ratio (BER), we can estimate the overall sensitivity of the microdisk photonic self-homodyne receiver. In this case the total RF input power that results in a baseband modulated optical power equal to the sensitivity of the digital photoreceiver is the minimum received power or the sensitivity of the wireless receiver.

Here we assume a single frequency baseband and an optimized RF modulation index of $m_1 = 0.8$. Fig. 38(a) shows the calculated receiver sensitivity against V_{HMM} for 3 different values of optical insertion loss. The optical input power ($P_{o,in}$) is 1 mW and the sensitivity of the photoreceiver is -40 dBm. Fig. 38(b) shows the calculated receiver sensitivity against optical input power ($P_{o,in}$) for two microdisk modulators with V_{HMM} of 0.45 V and 0.1 V. Again the sensitivity of the digital photoreceiver is -40 dBm. Fig. 38(c) shows the calculated receiver sensitivity against sensitivity of the digital photoreceiver. The optical input power ($P_{o,in}$) is 1 mW and V_{HMM} is 0.1 V. As may be seen a combination of low insertion loss (< 3dB), sensitive digital photoreceiver (<-65 dBm) and efficient photonic mixing (V_{HMM} < 0.2 V) results in a dramatic improvement in wireless receiver sensitivity (< -70 dBm).

With this sensitivity the microdisk photonic wireless receiver may be employed in high frequency carrier links such as LMDS[1]. For example EtherAir [2] that is a transceiver for LMDS has a sensitivity of –72 dBm at 26 GHz carrier frequency and –70 dBm at 38 GHz carrier frequency.

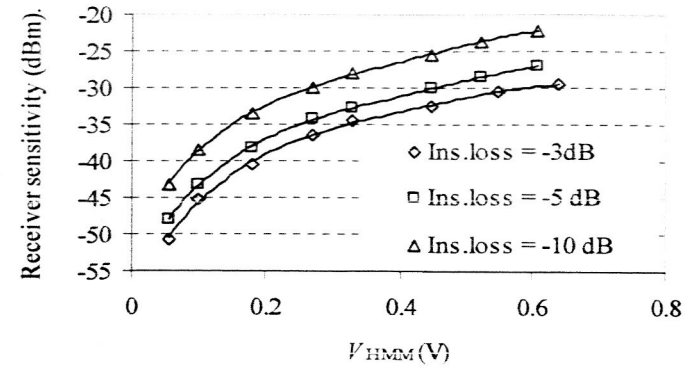

(a)

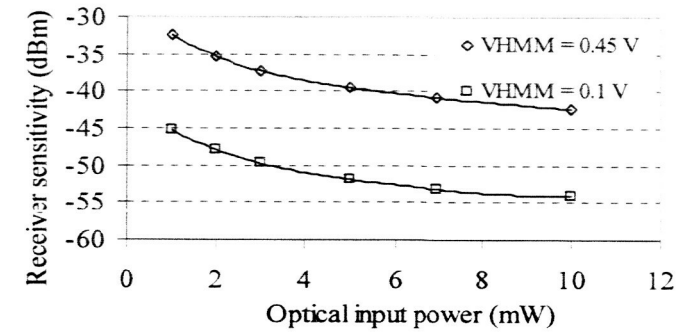

(b)

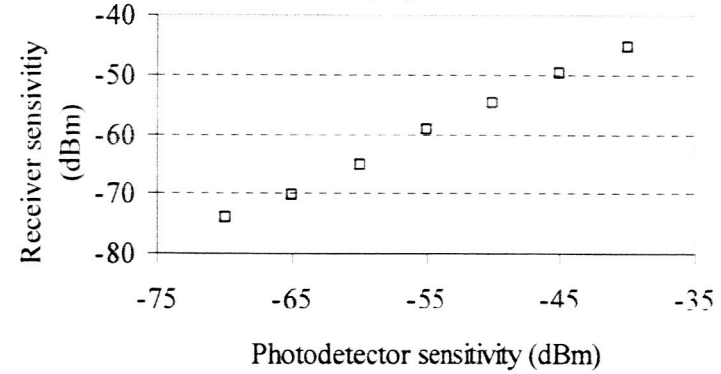

(c)

Figure 38 (a) Calculated receiver sensitivity against V_{HMM} for 3 different values of optical insertion loss (-10dB, -5 dB and -10 dB). The optical input power ($P_{o,in}$) is 1 mW and the sensitivity of the photoreceiver is -40 dBm. (b) Calculated receiver sensitivity against optical input power ($P_{o,in}$) for two microdisk modulators with V_{HMM} of 0.45 V and 0.1 V. The insertion loss is –3 dB. Again the sensitivity of the digital photoreceiver is -40 dBm. (c) Calculated receiver sensitivity against sensitivity of the digital photoreceiver for an optical input power ($P_{o,in}$) of 1 mW, insertion loss of –3 dB and V_{HMM} of 0.1 V.

The intensity of the modulating *E*-field inside the microdisk is proportional to the voltage gain factor (G_v) of the ring resonator and increases as the microdisk thickness (h) decreases.

The voltage gain factor can be improved by employing high quality RF-ring resonators but it will be limited by the RF loss in the ring and $LiNbO_3$ as well as the radiation losses. The simulation and experimental results show that by optimizing the surface quality of the ring resonator loaded RF-Qs of larger than 100 are achievable. The thinnest $LiNbO_3$ microdisk modulator reported so far has a thickness of 150 μm [15] but given the WG mode size and the possibility of fabricating toroidal $LiNbO_3$ microresonators, a thickness of 50 μm seems feasible. Reducing the microdisk thickness from 400 μm (the standard microdisk thickness used in most of our experiments) to 50 μm can increase the *E*-field intensity by a factor of 8.

Stability is one of the most important issues of the microdisk modulator that requires special attention. The linear or nonlinear modulation efficiency of the microdisk is very sensitive to the location of the laser wavelength relative to the resonant wavelength of the WG mode. The high quality factor of the WG modes makes the modulator extremely susceptible to thermal and mechanical fluctuations as well as the laser wavelength shift. We have demonstrated that applying a DC voltage on the ring resonator might be used to control the WG resonant wavelength through a feedback loop. The proof-of-concept experiment with a very basic feedback circuit shows that one can lock the laser wavelength to a specific location of the WG slope. This was achieved by comparing the photodetector output with a reference voltage and changing the DC bias voltage accordingly. A feedback loop that can guarantee steady sate operation over a long period of time requires a more sophisticated circuit design. As shown in Fig. 40 depending on desired operation regime of the microdisk modulator, the laser wavelength can be locked to different offset wavelengths relative to λ_{res}. In the case of nonlinear modulation, where the laser wavelength should be locked to λ_{res} (zero offset), the feed back loop should be able to determine the sign of the slope because deviation from λ_{res} to both directions generates the same amount of variation in optical output power.

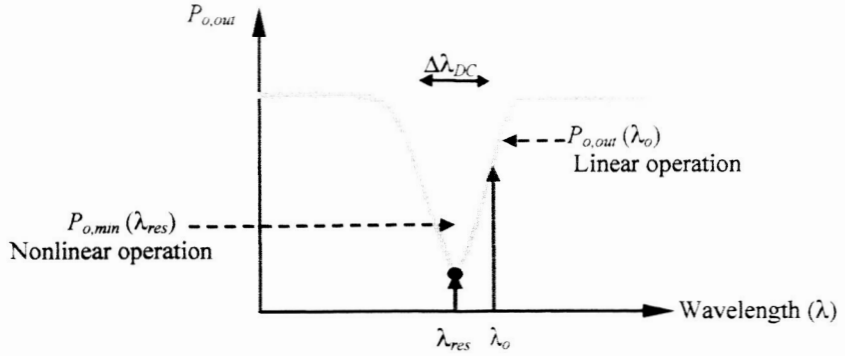

Figure 40 Relative alignment of the laser wavelength and WG resonant wavelength for linear and nonlinear modulation.

We can summarize the future challenges toward a more sensitive and stable microdisk modulator as follows:

1) Improved optical coupling.
2) Fabrication of very thin microdisks with high quality sidewalls.
3) High quality microring resonators.
4) Feed back circuit for wavelength locking.

In conclusion, if DNOM technique is used, employing a high sensitivity photoreceiver and post modulation optical filtering can increase the sensitivity of the photonic self-homodyne RF receiver. In DOF technique there is no high-frequency component in the optical intensity spectrum and filtering cann't remove the large DC component so the only possible modification is to enhance the performance of the photoreceiver.

Final design and integration

Fig. 41 shows the block diagrams of the microdisk photonic self-homodyne RF receiver. Here we summarize the desired specifications of each stage:

Laser: The laser should be a DFB laser with a very narrow linewidth and low *RIN*. Although a larger laser power results in a more efficient down-conversion but due to the small mode volume of WG resonances a high power density can cause thermal and nonlinear instabilities. The power threshold at which the modulator becomes unstable depends on the absorption and nonlinear characteristics of the electro-optic material used to fabricate the microdisk.

Optical waveguides: Low loss optical waveguides with the potential for integration with other photonic components is desired.

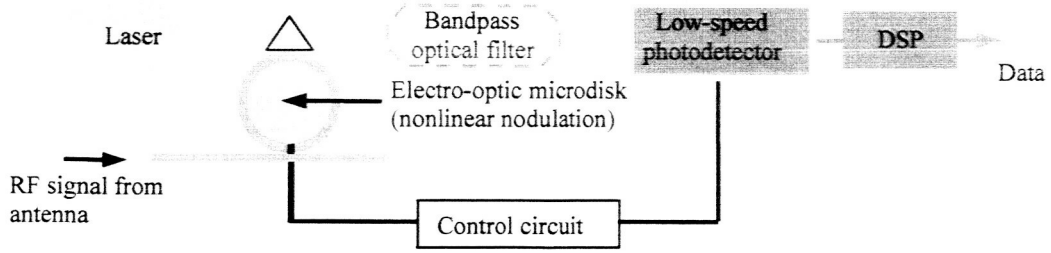

Figure 41 Schematic diagram of two microdisk photonic self-homodyne RF receiver architectures: (a) DNOM, where the microdisk is biased at nonlinear modulation regime and (b) DOF where the microdisk is biased at linear operating regime.

Optical filter: If we use DNOM technique, a bandpass optical filter with a bandwidth of less than $4f_{RF}$ helps the shot noise reduction (Fig. 42). For DOF technique a band-stop filter with a bandwidth larger than f_{RF} is a requirement for photonic down-conversion (Fig. 5.5(b)). In both cases the filter role-off is determined by the RF carrier frequency (f_{RF}) and the bandwidth of the baseband signal.

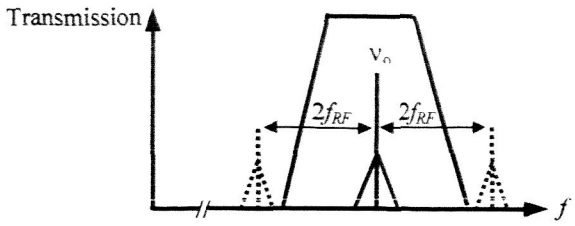

Figure 42 (a) Band pass filter in a DNOM photonic RF receiver decreases the shot noise by eliminating the high frequency components.

Recently multipole ring resonator based filter have been demonstrated with a very low loss and narrow passbands[3]. The role off of these filters can be increased by increasing the number of ring resonators (poles). Fig. 43(a) shows a photograph of a three-pole ring resonator filter and Fig. 43(b) shows the spectral response of multipole filters up to 6 poles[3].

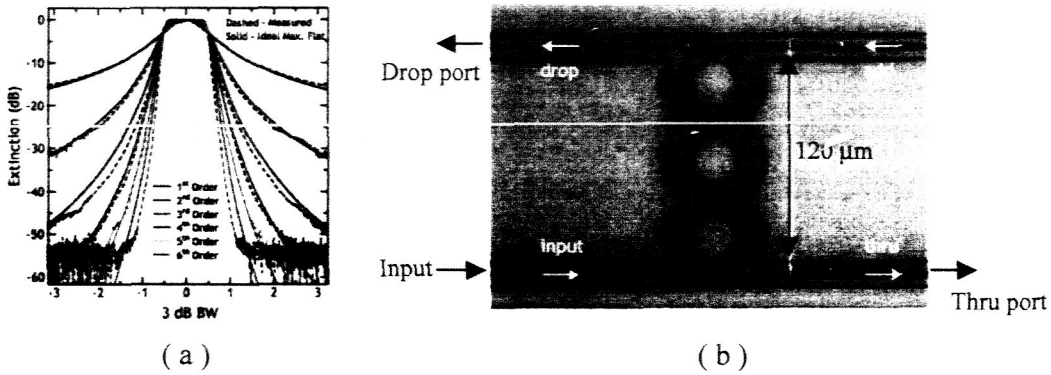

Figure 43 (a) Spectral response of optical filters with different number of ring resonator. (b) The multi ring resonator bandpass optical filter fabricated on *hydex* material system[3]

In order to clarify the benefits of using photonic technology in wireless receiver design here we make a crude comparison between a photonic receiver and an electronic receiver. A state-of-the-art 60 GHz superhetrodyne electronic receiver with a sensitivity of 10 µW (-20 dBm), consumes about 400 mW power (Ohata *et al. IEEE trans. on microwave theory and tech.*, 11(12), pp. 2354-2360, 1996). This receiver is built based on 0.15 µm N-AlGaAs/InGaAs HJFET MMIC technology and has a volume of 900 mm^3. The receiver consists of a low-noise amplifier (LNA), mixer and Local oscillator (LO). The local oscillator employs a dielectric resonator oscillator (DRO) that is co-integrated with a single-stage wide-band amplifier.

Thermal noise in the microdisk modulator, laser RIN noise and the photodetection noise generated by DC optical power are not considered in these simulations. A comprehensive noise analysis of the microdisk photonic receiver is a difficult task and is beyond the scope of the project.

However it is easy to show that post modulation optical filtering may improve the signal-to-noise ratio by reducing shot noise in the detector.
The shot noise in the photodetector is equal to $2eB(I_p+I_d)$, where I_d is the detector dark current, B is the detector bandwidth and I_p is the total amount of the total photocurrent (generated by the baseband modulated optical power and the DC optical power). We can write the mean square value of the noise photocurrents as:

$$i_N^2 = 2eB[I_p + R(P_{o,ac} + P_{o,dc})]$$

where $P_{o,dc}$ and $P_{o,ac}$ are the received DC and AC optical powers respectively. Due to low speed response of the photodetector the high-frequency components in the frequency spectrum of the optical output power (around $2f_{RF}$) do not contribute in the AC photocurrent. But these components can still generate shot noise. Therefore $P_{o,dc}$ is the sum of $P_{o,min}$ (transmitted optical power at resonance) the DC optical power and the modulated optical power at frequencies around $2f_{RF}$ (both generated through nonlinear modulation). For a critically coupled WG mode $P_{o,min}$ is zero but the DC and high-frequency components generated through mixing are always present.

Although the DC component cannot be eliminated, a band pass optical filter with a bandwidth less than $4f_{RF}$ can eliminate the high frequency optical components around 194 THz $\pm$ $2f_{RF}$ and cancel modulated optical power at $2f_{RF}$. Fig. 39 demonstrates the frequency domain signal flow in the presence of the optical filter.

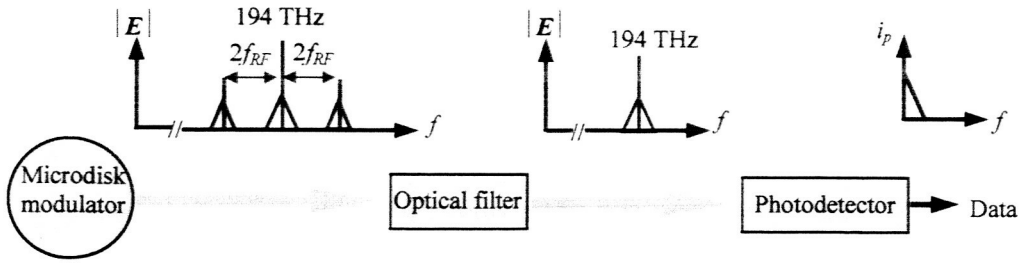

Figure 40 Schematic diagram of frequency signal flow in the photonic RF receiver in the presence of the optical filter.

The microdisk modulator is mainly determined by the optical quality factor and the intensity of the modulating E-field. The unloaded optical-Q is limited by the surface quality of the $LiNbO_3$ microdisk and the presence of the external particles on the sidewall. So a high quality polishing and a clean surface can improve the optical-Q. But we should keep in mind that the required bandwidth puts a fundamental limitation on the Q. So ideally we want to reach the bandwidth-limited regime, where the required bandwidth limits the Q, as opposed to surface-quality limited case. Optical coupling is also an important issue that affects the loaded optical-Q of the resonator as well as the unidirectional nature of the WG resonance. An ideal optical coupling mechanism should be lossless and have a negligible perturbing effect on the optical resonance.

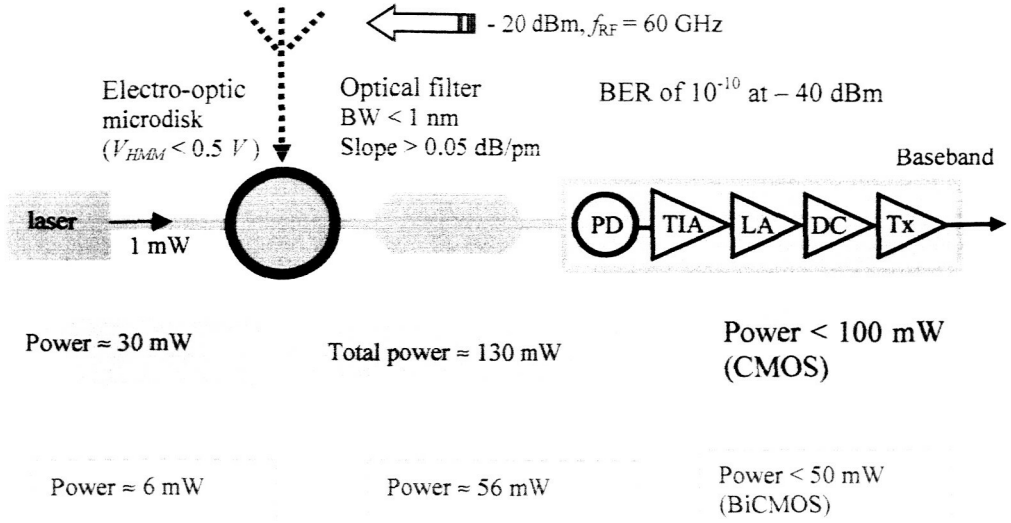

Figure 46 Estimated power consumption using commercially available technology (gray blocks), and costume design technology (dotted line).

Fig. 46 is the schematic diagram of a 60 GHz photonic self-homodyne receiver indicating the specification of each section and estimated power consumption.

Using a low cost laser source (about 3% power efficiency) and digital photoreceiver (based on CMOS technology) the estimated power consumption for a sensitivity of -20 dBm is about 130 mW. If we replace the laser with a more efficient laser (20%) and employ a low power photoreceiver based on BiCMOS technology the total power consumption is reduce to 56 mW. So photonic self-homodyne architecture can provide the same sensitivity while reducing the power consumption by a factor of 4 compared to an electronic receiver.
Beside low power consumption and better sensitivity the photonic receiver will benefit from the reduced size and complexity as well as low cost fabrication due to the absence of high-speed electronic components.

The estimated value of photonic receiver sensitivity (-20 dBm) is based on the current $LiNbO_3$ microdisk modulator technology, commercially available photoreceivers and a moderate input optical power (1 mW).

Due to versatility of the material and techniques used for fabricating different components in a photonic RF receiver, currently the most feasible approach for building an integrated system is hybrid integration on a silicon bench. Various silicon micromachining techniques that are originally developed for IC industry and MEMS devices can be employed to build features such as V-grooves and steps for mounting the photonic components. Fig. 47(a) shows schematic diagram an integrated $LiNbO_3$ microdisk photonic receiver based on hybrid integration technique. The $LiNbO_3$ microdisk, laser and the detector are mounted on pedestals with the proper height. The miniature ball lenses are aligned in a V-groove while the microprism is etched off the silicon substrate. Since silicon has a refractive index larger than $LiNbO_3$ (3.5 >

2.14) it can be used for evanescent optical coupling to the microdisk. Potentially the electronic circuitry including the signal processing and the control circuit can be fabricated directly on the silicon substrate.
In the future a monolithic fabrication process may be developed to build a fully integrated photonic receiver. For example lasers, detectors, waveguides, microring filters and also microdisk modulator have been already made based on compound semiconductor technology so in principle one may design a process sequence that allows monolithic integration of all these elements on the same substrate (Fig. 47(b)).

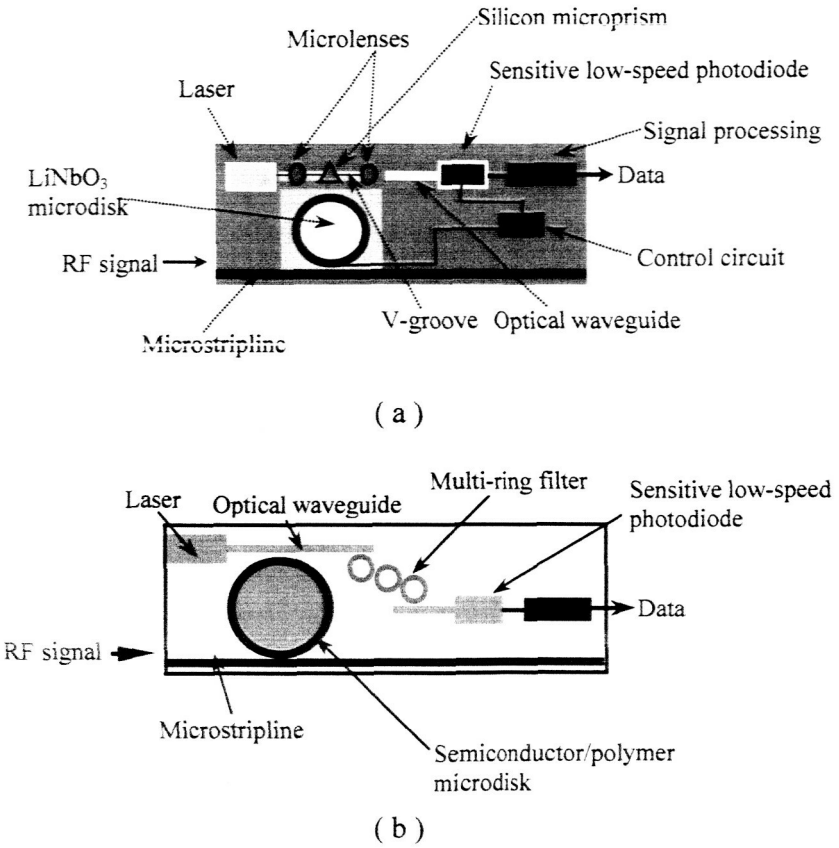

Figure 47 (a) Hybrid integration of a $LiNbO_3$ microdisk photonic RF receiver on a silicon bench. (b) Monolithic integration of a semiconductor microdisk photonic RF receiver based on compound semiconductor material system.

Conclusion

Results of analysis, modeling, device fabrication and measurement indicate that a microphotonic RF receiver is feasible. A novel self-homodyne photonic RF receiver based on a microdisk modulator has been developed. Down-conversion occurs in the optical domain through *nonlinear* modulation, thereby eliminating the need for an RF local oscillator and mixer. Experimental verification of the receiver architecture has been achieved by measuring BER and eye-diagrams using signals down-converted from a NRZ digital data modulated transmitted carrier RF signal with f_{RF} = 14.6 GHz carrier frequency. The microdisk modulator and the photonic self-homodyne architecture have the potential to be incorporated into a photonic integrated circuit by using alternative electro-optic materials (such as polymers and compound semiconductors). Reducing the disk diameter will extend the carrier frequency into mm-wave regime so that this receiver architecture has potential to be used in future indoor mm-wave wireless systems. The main challenges for future are

1) Improving the sensitivity of the microdisk modulator.
2) Designing more compact and efficient narrow band and directional planar antennas.
3) Reducing the size and a proper package design.
4) Increasing the carrier frequency to mm-wave regime.

Publications

In addition to quarterly technical reports, we have published a number of papers describing our work of both part I and part II of this research program [23-33].

References

[1] R. S. Weis and T. K. Gaylord, "Lithium Niobate: Summary of physical properties and crystal structure," *Appl. Phys. A*, Vol. 37, pp 191-203, 1985.

[2] W. M. Robetrtson, G. Arjavalingam, and G. V. Kopcsay, "Broadband microwave dielectric properties of $LiNbO_3$," *Electron. Lett.*, vol. 27, pp. 175-176

[3] K. K. Wong, "Properties of lithium niobate," *ISPEC*, institution of electrical engineers, 1989.

[4] A. M. Prokhov and Y. S. Kuz'minov, "Physics and chemistry of crystalline lithium niobate," The Adam Hilger series on optics and optoelectronics, 1990.

[5] B. Little, J. P. Laine, H. A. Haus, "Analitic theory of coupling from tapered fibers and half-blocks into microsphere resonators", *J. of Lightwave Technol.*, Vol. 17, No. 4, pp 704-714, April 1999.

[6] S. Schiller and R. L. Byer, "High-resolution spectroscopy of whispering gallery modes in large dielectric spheres", *Optics Lett.*, Vol. 16, No. 15, pp 1138-1440, Aug. 1991.

[7] M. L. Gorodetsky and V. S. Ilchenko, "High-Q optical whispering-gallery microresonators:precession approach for spherical mode analysis and emission patterns with prism couplers", Optics comm., Vol. 113, pp 133-143, Dec. 1994.

[8] T. Ikegami and K. Kubodera, "Nonlinear optical devices for switching applications", Communications, 1990. ICC 90 IEEE international conference on, Vol. 3, pp 1152-1156, Apr.

[9] P. W. Smith, E. H. Turner, and P. J. Maloney, "Electro-optic nonlinear Fabry-Perot devices", *IEEE J. of quanum electron.*, Vol. 14, No. 3, pp 207-212, March 1978.

[10] R. S. Jameson and W. T. Lee, " Operation of an all-optical bistable device dependent upon incident and transmitted optical power", *IEEE J. of quantum electron.*, Vol. 25, No. 2, pp 139-143, Feb. 1989.

[11] I. L. Gheorma and R. M. Osgood, Jr., "The fundamental limitations of optical resonator based high-speed EO modulators," *IEEE Photon. Technol.*, vol. 14, no. 14, pp. 795-797, June 2002.

[12] Y. S. Wu, and F. J. Rosenbaum, " Mode chart for microstrip ring resonators ", *IEEE trans. on microwave theory and techniques*, Vol. MTT-21, pp 487-489, July 1973.

[13] A. Khanna, and Y. Garault, "Determination of loaded, unloaded, and external quality factors of a dielectric resonator coupled to a microstripline", *IEEE trans. on microwave theory and techniques*, Vol. MTT-31, No 3, pp 261-264, March 1993.

[14] S.-L. Lu, and A. M. Ferendeci, " Coupling parameters for a side-coupled ring resonator and a microstrip line ", *IEEE trans. on microwave theory and techniques*, Vol. 44, No. 6, pp 953-956, June 1996.

[15] V. S. Ilchenko, A. A. Savchenkov, A. B. Matsko, and L. Maleki, "Sub-microwatt photonic microwave receiver", *IEEE photonics technol.*, Vol 14, No. 11, Nov 2002.

[16] B. Vidal, V. Polo, J. L. Corral, and J. Marti, "Efficient architecture for WDM photonic microwave filters," *IEEE Photon. Technol. Lett.*, vol. 16, pp. 257-259, Jan. 2004.

[17] P. O. Hedekvist, B.-E. Olsson, and A. Wiberg, "Microwave harmonic frequency generation utilizing the properties of an optical phase modulator," *J. Lightwave Technol.*, vol. 22, pp. 882-886, March 2004.

[18] Hirata, M. Harada, and T. Nagatsuma, "120-GHz wireless link using photonic techniques for generation, modulation, and emission of millimeter-wave signals," *J. Lightwave Technol.*, vol. 21, pp. 2145-2153, Oct. 2003.

[19] G. K. Gopalakrishnan, W. K. Burns, and Catherine H. Bulmer, "Microwave-optical mixing in $LiNbO_3$ modulators," *IEEE Trans. Microwave Theory and Tech.*, vol. 41, pp. 2383-2391, Dec 1993.

[20] M. Tsuchiya and T. Hoshida, "Nonlinear photodetection scheme and its system applications to fiber-optic millimeter-wave wireless down-links," *IEEE Trans. Microwave Theory and Tech.*, vol. 47, pp. 1342-1350, July 1999.

[21] A. A. Abidi, "Direct-conversion radio transceivers for digital communications," *IEEE J. Solid-State Circuits*, vol. 30, pp 1399-1410, Dec 1995.

[22] Y. Shoji, K. Hamaguchi, H. Ogawa, "Millimeter-wave remote self-heterodyne system for extremely stable and low cost broad-band signal transmission", *IEEE Trans. Microwave. Theory and Tech*, vol. 50, pp1458-1468, June 2002.

[23] M. Hossein-Zadeh, A. F. J. Levi, "14.6 GHz $LiNbO_3$ microdisk photonic self-homodyne RF receiver," submitted to *Journal of Light Wave Technology*, April 2004.

[24] M. Hossein-Zadeh, A. F. J. Levi, "Self-homodyne RF-optical $LiNbO_3$ microdisk receiver," accepted to be published in *Solid-State Electronics*.

[25] M. Hossein-Zadeh, A. F. J. Levi, "RF Mixing in $LiNbO_3$ microdisk modulator," *IEEE/LEOS summer topical meetings*, 2004, section MC4: WGM microcavities IV.

[26] M. Hossein-Zadeh, A. F. J. Levi, "Self-Homodyne RF-Optical $LiNbO_3$ microdisk receiver," *Technical digest CLEO conference*, 2004, Microwave photonics session, CWQ5.

[27] M. Hossein-Zadeh, A. F. J. Levi, "Self-Homodyne RF-Optical $LiNbO_3$ microdisk receiver," *GOMACTech-04 conference*, 2004.

[28] M. Hossein-Zadeh, A. F. J. Levi, "A new electrode design for microdisk electro-optic RF modulator," *Technical digest CLEO conference*, 2003, CTuW3.

[29] M. Hossein-Zadeh, F. Harriague, A. F. J. Levi, "Mb/s data transmission over an RF-Optical-link using a LiNbO3 microdisk optical modulator," *Technical digest CLEO conference*, 2002, pp 277.

[30] M. Hossein-Zadeh, A. F. J. Levi, "Mb/s data transmission over a RF fiber-Optic link using a LiNbO3 microdisk optical modulator," *Solid-State Electronics*, 46, 2173-2178, 2002.

[31] D.A. Cohen, M. Hossein-Zadeh, A. F. J. Levi, "High-Q microphotonic electro-optic modulator," *Solid-State Electronics*, 45, 1577-1589, 2001.

[32] D.A. Cohen, M. Hossein-Zadeh, A. F. J. Levi, "Microphotonic modulator for microwave receiver," *Electronics Letters*, 37, 300-301, 2001.

[33] D. A. Cohen and A. F. J. Levi, "Microphotonic millimeter-wave receiver architecture," *Electron. Lett.*, 37, 37-39, 2001.

[34] D. A. Cohen and A. F. J. Levi, "Microphotonic components for a mm-wave receiver," *Solid State Electron.*, 45, 495-505, 2001.

[35] D. A. Cohen, "Lithium Niobate microphotnic modulators" , Ph.D dissertation, USC May 2001.

[36] M. Hossein-Zadeh, "Electro-optic microdisk wireless photonic receiver", PhD dissertation, USC, Dec 2004.

Notes

(1) LMDS (Local Multipoint Distribution Service) is a fixed wireless technology that operates in the 26 – 32 GHz band and offers line-of-sight coverage over distances up to 3-5 Klm.

(2) EtherAir 1500: is a digital radio system made by Ceragon networks that supports wireless fast Ethernet applications for the ISP carrier, corporate access and campus environments. This system operates in the 18,23,26,28 and 38 GHz frequency bands with a bandwidth of 155 Mbps. (www.ceragon.com).

(3) Little optics (http://www.littleoptics.com)